Dalton Transactions

PAPER

View Article Online
View Journal | View Issue

Cite this: *Dalton Trans.*, 2014, **43**, 3313

Induced chirality-at-metal and diastereoselectivity at Δ/Λ-configured distorted square-planar copper complexes by enantiopure Schiff base ligands: combined circular dichroism, DFT and X-ray structural studies†

Mohammed Enamullah,*[a] A. K. M. Royhan Uddin,[a] Gennaro Pescitelli,*[b] Roberto Berardozzi,[b] Gamall Makhloufi,[c] Vera Vasylyeva,[c] Anne-Christine Chamayou[d] and Christoph Janiak*[c]

Bidentate enantiopure Schiff base ligands, (*R* or *S*)-*N*-1-(Ar)ethyl-2-oxo-1-naphthaldiminato-κ^2*N*,*O*, diastereoselectively yield Δ/Λ-chiral four-coordinated, non-planar Cu(*N*^*O*)$_2$ complexes [Ar = C_6H_5 ***R***/***S***-**L1**, *m*-C_6H_4OMe ***R***-**L2**, *p*-C_6H_4OMe ***R***/***S***-**L3**, and *p*-C_6H_4Br ***R***/***S***-**L4**]. Two *N*,*O*-chelate ligands coordinate to the copper(II) atom in distorted square-planar mode, and induce metal-centered Δ/Λ-chirality at the copper atom in the C_2-symmetric complexes. In the solid state, the ***R***-**L1** (or ***R***-**L4**) ligand chirality diastereoselectively induces a Λ-Cu configuration in **Λ-Cu-*R*-L1** (or **Λ-Cu-*R*-L4**), the ***S***-**L1** ligand a Δ-Cu configuration in **Δ-Cu-*S*-L1**, forming enantiopure crystals upon crystallization. Conversely, the ***R***-**L2** ligand combines both **Λ/Δ-Cu-*R*-L2** as a diastereomeric pair in the crystals. In solution, electronic circular dichroism (CD) spectra show full or partial diastereoselectivity towards Λ-Cu for *R* ligands and towards Δ-Cu for *S* ligands. The electronic CD spectra measured on all complexes obtained from *R* ligands (or *S* ligands), *e.g.* **Cu-*R*-L1**, **Cu-*R*-L2**, **Cu-*R*-L3**, and **Cu-*R*-L4** (or **Cu-*S*-L1**, **Cu-*S*-L3**, and **Cu-*S*-L4**), show consistent spectral features. TDDFT calculations of the electronic CD spectra for the diastereomers **Λ-Cu-*R*-L1** and **Δ-Cu-*R*-L1** suggest that the CD spectra are largely dominated by the configuration at the metal center (**Λ** *vs.* **Δ**). The experimental CD spectrum of **Cu-*R*-L1** agrees well with the one calculated for the **Λ-Cu-*R*-L1** configuration. Cyclic voltammetry of **Cu-*R*-L1** reveals a quasi-reversible redox wave corresponding to one-electron transfer for the $[Cu^{II}L_2]^0/[Cu^{I}L_2]^{-1}$ couple in acetonitrile. DSC analyses for the complexes show an exothermic peak between 377 and 478 K (ΔH = −12 to −43 kJ mol^{-1}), corresponding to a phase transformation from distorted square-planar/tetrahedral to regular tetrahedral geometry on heating.

Received 11th October 2013,
Accepted 27th November 2013

DOI: 10.1039/c3dt52871e

www.rsc.org/dalton

Introduction

Syntheses, stereoselectivity and molecular structures of divalent transition metal complexes with chiral *N*^*O* chelate Schiff-base ligands are of continued interest[1–10] and have been used efficiently as chiral catalysts.[1*l*,*m*,9,11–15] We have recently investigated the syntheses, stereochemistry, and molecular structures of Rh(η^4-cod)-complexes containing chiral bidentate *N*,*O*-chelate Schiff base ligands.[16,17] Four-coordinated metal compounds with two asymmetrical bidentate ligands exhibiting tetrahedral to distorted square-planar geometry are chiral, and the helical chirality of the whole coordination unit may be indicated with Δ and Λ descriptors.[18*a*] Here, two identical *N*^*O* chelate ligands afford C_2-symmetrical metal complexes with metal-centered helical Λ- or Δ-chirality (Scheme 1).[18*b*,*c*]

[a]*Department of Chemistry, Jahangirnagar University, Dhaka 1342, Bangladesh. E-mail: enamullah@juniv.edu*
[b]*Department of Chemistry, University of Pisa, via Risorgimento 35, 56126 Pisa, Italy. E-mail: ripes@dcci.unipi.it*
[c]*Institut für Anorganische Chemie und Strukturchemie, Universität Düsseldorf, Universitätsstr. 1, D-40225 Düsseldorf, Germany. E-mail: janiak@uni-duesseldorf.de*
[d]*Institut für Anorganische and Analytische Chemie, Universität Freiburg, Albertstr. 21, D-79104 Freiburg, Germany*

† Electronic supplementary information (ESI) available: Listings of EI and APCI mass spectral data, polarimetric data, additional ^{1}H-NMR spectra, additional packing diagrams, calculated UV-vis/CD spectra for single structures, additional calculation details, and CIF files reported in this paper. CCDC 962481–962487. For ESI and crystallographic data in CIF or other electronic format see DOI: 10.1039/c3dt52871e

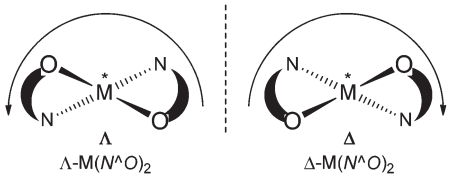

Scheme 1 Enantiomeric absolute configurations of a non-planar bis-chelate complex viewed along the C_2 axis: Λ left-handed helicity, Δ right-handed helicity along the principal C_2 axis (perpendicular to the paper plane). *N* and *O* convey the chelate ring asymmetry.

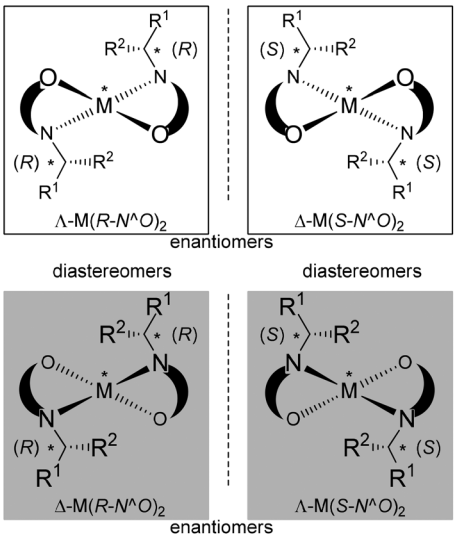

Scheme 2 Enantiomeric and diastereomeric Δ/Λ-[M(*R*/*S*-*N*^*O*)$_2$] pairs. The position of the *R*- or *S*-stereogenic center on the branched α-carbon of the N substituent is adapted in the present work (see Scheme 3) but could also reside in or on the *N*^*O* chelate handle. The priority for the *R*- or *S*-assignment is assumed to be N > R^1 > R^2. In the present work Λ-metal-*R*-ligand complexes and Δ-metal-*S*-ligand complexes in the white boxes are the major combinations. The opposite and here minor Δ-metal-*R*-ligand complexes and Λ-metal-*S*-ligand combinations are underlined in gray.

Consequently, enantiopure *R*- or *S*-*N*^*O* chelate ligands can lead to diastereomeric pairs of the type Λ-M-*R*-*N*^*O* and Δ-M-*R*-*N*^*O* (or Δ-M-*S*-*N*^*O* and Λ-M-*S*-*N*^*O*), while racemic *R*/*S*-*N*^*O* ligands give all four isomers (Scheme 2). Intramolecular non-covalent interactions acting within the metal–chiral chelate complexes lead to a free-energy difference between the diastereomers, thereby one of the two possible diastereomers may be formed preferentially (Scheme 2).[6,7,19–22]

Some examples of such diastereoselection in tetrahedral to near-square-planar complexes of the type [M(*R*- or *S*-*N*^*O*)$_2$] (M = Co, Cu, Ni, Zn) with predominant formation of Λ- or Δ-configuration, evidenced by X-ray studies and circular dichroism (CD) spectra in solution, have been reported.[6,7,19–22] The diastereoselection seemed quantitative in the solid state based on a single-crystal X-ray study while solution investigations by ^{1}H-NMR and vibrational CD (VCD) spectroscopy showed the existence of both Λ- and Δ-diastereomers with a ratio of *ca.* 80 : 20 for bis[{(*R* or *S*)-*N*-(Ar)ethyl-salicylaldiminato-κ^2*N*,*O*}]-Zn(II)[19] or 67 : 33 for bis[{(*R* or *S*)-2-(2-hydroxy-1-phenylethyl-imino)methyl-phenolato-κ^2*N*,*O*}]Zn(II).[21a] However, very few examples of such diastereoselection in near-square-planar complexes Cu(*R*-*N*^*O*)$_2$ (*N*^*O* = (*R*)-*N*-(phenyl)ethyl-X-salicylaldiminate) with the formation of, *e.g.*, Δ-Cu-*R*-*N*^*O* configuration[7a,c,e] or Λ-Cu-*R*-*N*^*O* configuration[7e,f] have been reported based on X-ray studies.

In the above examples, the diastereomeric ratio depends on the thermodynamics of stereochemical induction by the ligand. This mechanism is well studied for octahedral[18,23] or five-coordinated complexes[24] but little research activity has been invested in the diastereoselection of four-coordinate, asymmetric complexes. For the latter, the Δ- or Λ-configuration can interconvert by ligand exchange or in particular by rearrangement through a planar geometry. In order to study the diastereoselection phenomenon, the choice of method is important for determining both the absolute configuration and the diastereomeric composition. X-ray single crystallography appears to be a straight-forward method for determination of the metal-centered absolute configuration.[25,26] The solid state structure, however, does not necessarily represent the thermodynamically most stable geometry in solution or in the gas phase. During the crystallization process various intermolecular contacts and lattice forces become important, which can shift the equilibrium between Δ- and Λ-geometry at the metal ion, possibly even leading to inversion of the absolute metal configuration from solution to the solid state. Furthermore, usually only one single crystal is used for structure determination and this does not rule out formation of a diastereomeric conglomerate. Just like the better known *racemic conglomerate*[27] we describe here a diastereomeric conglomerate as a mixture of crystals where each one contains only one of the two diastereomers from a diastereomeric pair. In this case, no quantitative information about stereochemical induction can be drawn from the crystal structure.

In order to obtain reliable results about the Δ/Λ-equilibrium in solution in a minimal invasive way, *i.e.* avoiding molecular interactions with reagents, chromatography columns *etc.*, it is necessary to use spectroscopic methods. The equilibrium between two diastereomers can be easily studied using nuclear magnetic resonance (NMR). Integration of characteristic signals with different chemical shifts for the Δ- and the Λ-diastereomer readily delivers the diastereomeric ratio. This approach, however, does not allow assignment of the absolute configuration of each diastereomer and is hampered for paramagnetic Cu(II) complexes. The absolute configuration can be obtained using chiroptical spectroscopy, in particular electronic circular dichroism (CD), especially with the support of theoretical calculations.[28] Circular dichroism is the differential absorbance of left minus right circularly polarized light. Thus, the sign of the obtained bands is characteristic of the absolute configuration of the molecule, while the overall spectrum profile depends on the overall stereochemistry, including configuration and conformation.[29] Electronic CD (ECD or simply CD), which detects the differential

absorbance of visible or UV-light, is applicable to molecules combining one or more chromophores, having observable electronic transitions, with at least one chirality element. For chiral transition metal complexes these could be either ligand transitions or d–d transitions of the metal ion.[30]

We report here the syntheses, characterization, solid-state structures, solution CD and theoretical studies of Λ- or Δ-bis[{(*R* or *S*)-*N*-(Ar)ethyl-2-oxo-1-naphthaldiminato-κ^2*N*,*O*}]-copper(II). These complexes exhibit non-planar structures involving a chiral copper ion. (*R* or *S*)-Ligand chirality induces diastereoselection of the Λ- or Δ-metal configuration in the solid state and dynamic diastereomeric equilibria (Λ *vs.* Δ) occur in solution.

Results and discussion

The reaction of enantiopure (*R* or *S*)-*N*-1-(Ar)ethyl-2-oxo-1-naphthaldimine with copper(II)acetate provides the Λ- or Δ-bis-[{(*R* or *S*)-*N*-(Ar)ethyl-2-oxo-1-naphthaldiminato-κ^2*N*,*O*}]copper(II) complexes (Scheme 3). The characteristic νC=N bands for the imine group of coordinated Schiff bases are found at 1617–1604 cm^{-1} in the complexes.[16a,c,19,21] The complexes **Cu-*R*-L1** to **Cu-*R*-L4** react with KCN to give diamagnetic $[Cu(CN)_4]^{3-}$ and deprotonated Schiff base (L^-) species in the reaction mixture (monitored by ^{1}H NMR, see ESI†), accompanied by a color change from brown to red-orange.

EI and APCI mass spectra show the expected parent ion and ligand peaks (Table S1 in ESI†). The optical rotations $[\alpha]_D$ of *R*-HL1 and *S*-HL1 as well as the complexes obtained thereof are in opposite directions, as expected (Table S2 in ESI†).

Thermally induced structural phase transition

Thermally induced structural phase transition has been reported for related Cu(II)-/Ni(II)-chiral *N*,*O*-chelate complexes[7a–d,31] accompanying a change from a square-planar (or distorted tetrahedral) to regular tetrahedral environment on heating from room temperature. The DSC curves of heating for the complexes show an exothermic peak between 377 and 478 K (ΔH = −12 to −43 kJ mol^{-1}) (Table 1). This structural phase transition, in analogy with related complexes,[7a–d,31] corresponds to a phase transformation from a distorted square-planar/tetrahedral to regular tetrahedral geometry on heating.

Table 1 Thermally induced structural phase transformation data for the complexes

Compound	Peaks (K)/ΔH (kJ mol^{-1}) (powder form)	Peaks (K)/ΔH (kJ mol^{-1}) (single crystals)
Cu-*R*-L1	478/−33.6	478/−24.8
Cu-*S*-L1	476/−29.3	478/−25.3
Cu-*R*-L2		389/−25.5
Cu-*S*-L3	377/−12.3	
Cu-*R*-L4		460/−42.7

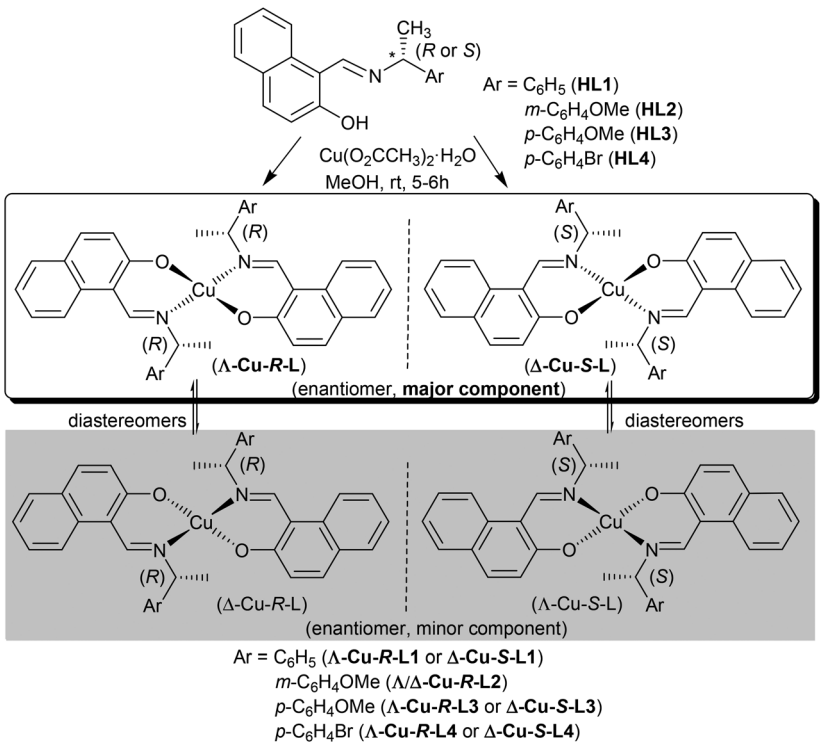

Scheme 3 Synthetic route to Λ- or Δ-bis[{(*R* or *S*)-*N*-(Ar)ethyl-2-oxo-1-naphthaldiminato-κ^2*N*,*O*}]copper(II). The Λ-Cu-*R*-ligand and Δ-Cu-*S*-ligand complexes in the white box are the major combinations. The opposite and here the minor Δ-Cu-*R*-ligand and Λ-Cu-*S*-ligand combinations are underlined in gray (*cf.* Scheme 2).

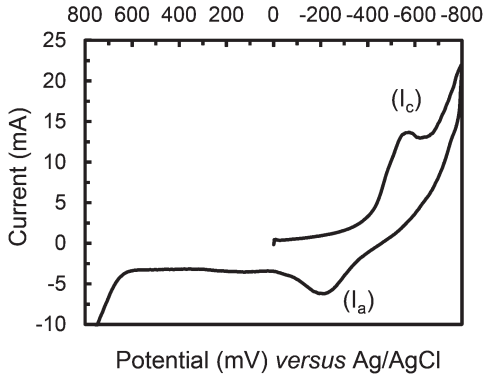

Fig. 1 Cyclic voltammogram of **Cu-*R*-L1** (0.5 × 10^{-3} mol dm^{-3}) containing TBAP (0.1 mol dm^{-3}) at a platinum electrode, scan rate of 150 mV s^{-1} at 298 K in acetonitrile.

Cyclic voltammetry

The cyclic voltammograms of **Cu-*R*-L1** were recorded in the range of 800 to −1100 mV *versus* Ag/AgCl, using several switching potentials at varying scan rates. The voltammogram shows, during the reduction scan (0.0 mV to −800 mV), a cathodic peak I_c at −575 mV corresponding to the first electron transfer for the reaction $[Cu^{II}(L1)_2]^0$ to $[Cu^{I}(L1)_2]^{-1}$ (Fig. 1). On the oxidation scan the reversibility of waves I_c is illustrated by the presence of the corresponding anodic peak I_a at −214 mV. The second electron transfer assigned to the $[Cu^{I}(L1)_2]^-$/$[Cu^{0}(L1)_2]^{-2}$ couple is not detected due to the overlap with the cathodic decomposition of the electrolytic medium over switching potential at around −700 mV. Analysis of voltammograms at varying scan rates (80, 100, 120, and 150 mV s^{-1}) demonstrates that the peak current ratio of I_a/I_c decreases at faster scan rates.[32] The voltammetric results strongly support a quasi-reversible one electron charge transfer corresponding to the Cu^{II}/Cu^{I} couple as found for related copper(II)–Schiff base complexes.[32,33]

Solid state structural studies

The copper atoms in the complexes synthesized here with the ligands **L1** to **L4** have a four-coordinate structure as evidenced by single crystal X-ray determinations of **Cu-*R*-L1**, **Cu-*S*-L1**, **Cu-*R*-L2** and **Cu-*R*-L4**. For ligands **L1** and **L2** the two *N*^*O*-bidentate Schiff base ligands form a non-planar N_2O_2-coordination sphere around the copper atom which is distorted from square-planar (Fig. 2 and 3, Table 2). For the *p*-bromophenyl ligand **L4** the copper coordination sphere is very close to square-planar with only a small distortion towards the Λ-configuration (Fig. 4, Table 2). The Cu–O and Cu–N lengths and bond angles in the complexes are listed in Table 2 and are as expected from literature reports for similar Cu(II) complexes.[33a,34]

Visual inspection of the molecular structures in Fig. 2 and 3 already shows that the four-coordinated bis-chelate copper complexes deviate substantially from a square-planar configuration around the Cu(II) metal atom. Quantitatively, the degree of distortion from square-planar can be expressed by the dihedral angle θ between the two planes formed by the donor atoms with the metal atom, that is, N1–M–O1 and N2–M–O2 (Scheme 4 and Table 3). This dihedral angle is 90° for tetrahedral geometry and 0° for square-planar geometry (not

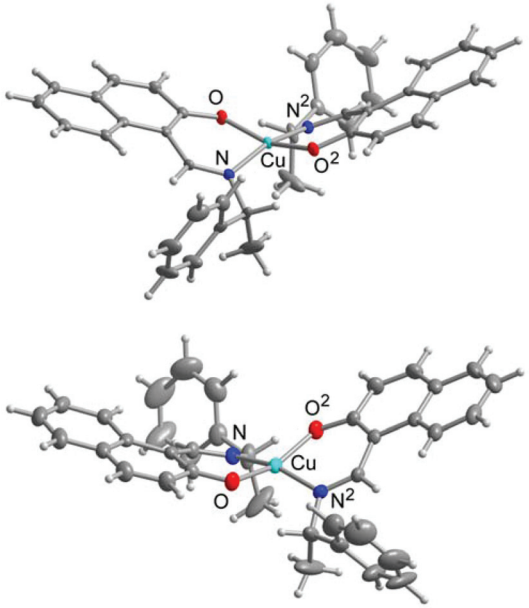

Fig. 2 Molecular structures of **Λ-Cu-*R*-L1** (top, low temperature data set CuRL1a) and **Δ-Cu-*S*-L1** enantiomer (bottom, data set CuSL1-III) (50% thermal ellipsoids for non-hydrogen atoms). See Table 2 for bond lengths and angles.

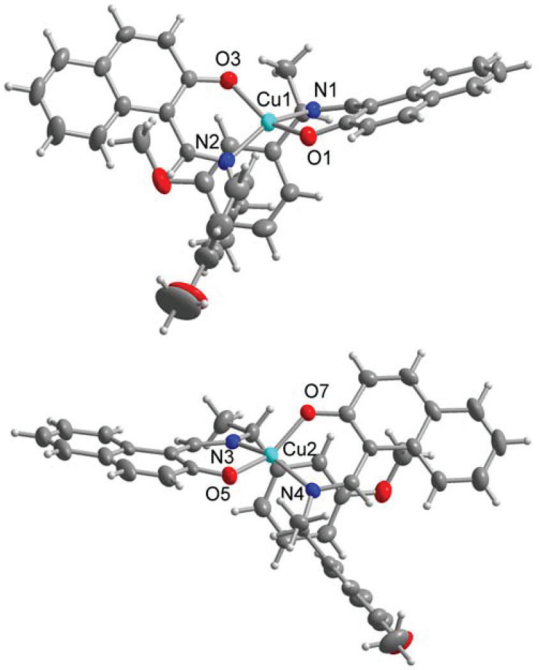

Fig. 3 Molecular structures of **Λ/Δ-Cu-*R*-L2**. There are two symmetry independent molecules in asymmetric unit forming a diastereomeric pair, Cu1 has Λ- and Cu2 has Δ-configuration (50% thermal ellipsoids for non-hydrogen atoms). See Table 2 for bond lengths and angles.

Table 2 Selected bond lengths (Å) and angles (°) in Λ-Cu-*R*-L1, Δ-Cu-*S*-L1, Λ/Δ-Cu-*R*-L2, and Λ-Cu-*R*-L4

Λ-Cu-*R*-L1[a]			
Two different crystals: data set CuR12 (top) and CuRL1a (bottom)			
Cu–O	1.894(2)	O–Cu–N	91.72(12)
	1.9061(16)		91.76(8)
Cu–N	1.958(3)	O–Cu–N^2	91.29(12)
	1.9632(19)		91.22(8)
		O–Cu–O^2	159.05(15)
			159.25(10)
		N–Cu–N2^2	163.38(16)
			163.29(11)
Δ-Cu-*S*-L1[a]			
Two different crystals: data set CuSL1-II (top) and CuSL1-III (bottom)			
Cu–O	1.903(4)	O–Cu–N	91.61(18)
	1.893(2)		91.65(11)
Cu–N	1.963(5)	O–Cu–N^2	91.55(18)
	1.960(3)		91.70(11)
		O–Cu–O^2	158.95(3)
			158.22(17)
		N–Cu–N2^2	162.7(3)
			162.19(18)
Λ-Cu-*R*-L2			
Two different crystals: data set CuR14a (top) and CuRL2-LT (bottom)			
Cu1–O1	1.886(3)	O3–Cu1–N2	93.63(14)
	1.886(4)		93.52(16)
Cu1–O3	1.890(3)	O1–Cu1–N1	92.00(14)
	1.887(3)		92.44(16)
Cu1–N1	1.962(4)	O3–Cu1–N1	99.26(14)
	1.953(4)		99.20(16)
Cu1–N2	1.932(4)	O1–Cu1–N2	93.31(14)
	1.931(4)		93.34(16)
		O3–Cu1–O1	144.39(13)
			144.44(15)
		N2–Cu1–N1	149.61(14)
			149.12(16)
Δ-Cu-*R*-L2			
Two different crystals: data set CuR14a (top) and CuRL2-LT (bottom)			
Cu2–O5	1.895(3)	O5–Cu2–N3	93.37(14)
	1.901(3)		93.15(16)
Cu2–O7	1.898(3)	O7–Cu2–N4	93.51(14)
	1.903(3)		93.56(15)
Cu2–N3	1.948(4)	O5–Cu2–N4	94.81(14)
	1.950(4)		95.05(16)
Cu2–N4	1.946(4)	O7–Cu2–N3	94.47(14)
	1.953(4)		94.38(16)
		O5–Cu2–O7	149.60(12)
			149.83(14)
		N3–Cu2–N4	148.83(14)
			148.62(16)
Λ-Cu-*R*-L4			
Cu–O1	1.860(2)	O1–Cu–O2	177.09(9)
Cu–O2	1.868(2)	O1–Cu–N1	89.05(9)
Cu–N1	1.995(2)	O1–Cu–N2	90.59(9)
Cu–N2	1.993(2)	O2–Cu–N1	90.79(9)
		O2–Cu–N2	89.71(9)
		N1–Cu–N2	177.35(10)

[a] Symmetry code 2 = 1 − *x*, 1 − *y*, *z*.

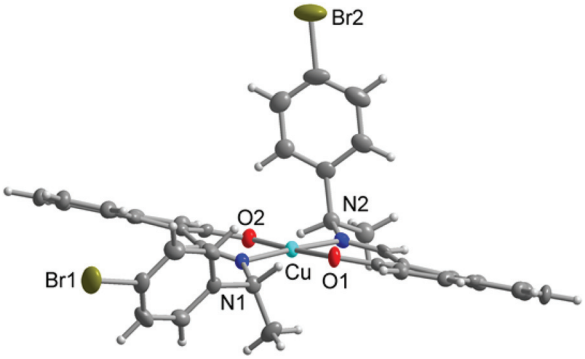

Fig. 4 Molecular structure of Λ-Cu-*R*-L4 (70% thermal ellipsoids for non-hydrogen atoms). See Table 2 for bond lengths and angles.

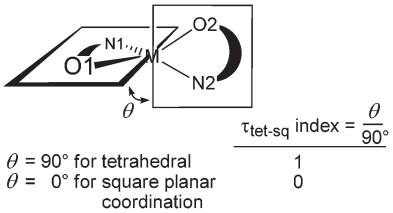

Scheme 4 Assessment of deviations between tetrahedral and square-planar geometry by the dihedral angle θ or the $\tau_{\text{tet-sq}}$ index.

Table 3 Measure of distortions from square-planar metal geometry

Compound	θ^a/°	$\tau_{\text{tet-sq}} = \theta/90°$	$\tau_4{}^b$
Λ-Cu-*R*-L1			
Data set CuR12	26.5(1)	0.29	0.27
CuRL1a	26.27(6)	0.29	0.27
Δ-Cu-*S*-L1			
Data set CuSL1-II	27.0(2)	0.30	0.27
CuSL1-III	27.9(1)	0.31	0.28
Λ-Cu(1)-*R*-L2			
Data set CuR14a	46.07(3)	0.51	0.47
CuRL2-LT	46.3(1)	0.51	0.47
Δ-Cu(2)-*R*-L2			
Data set CuR14a	42.8(1)	0.48	0.44
CuRL2-LT	42.8(1)	0.48	0.44
Λ-Cu-*R*-L4	3.88(7)	0.04	0.04

[a] Calculated using Diamond[38] based on the planes formed by the N–Cu–O chelate. [b] Defined as in ref. 36. See Table 2 for the two largest angles α and β.

considering the distortion induced by the chelate ring formation).[35] Angle θ can be normalized through division by 90° (θ/90°) to give an index $\tau_{\text{tet-sq}}$ = 1 for tetrahedral and 0 for square-planar geometry, respectively (Scheme 4).

Furthermore, a geometry index τ_4 for four-coordinate complexes with $\tau_4 = [360° - (\alpha + \beta)]/141°$ has been proposed,[36] similar to Addison and Reedijk's five-coordinate τ_5 index,[37]

with α and β as the two largest angles (N–Cu–N and O–Cu–O) in the four-coordinate species. The values of τ_4 will range from 1 for a perfect tetrahedral geometry, since 360 − 2(109.5) = 141, to 0 for a perfect square-planar geometry, since 360 − 2(180) = 0. Structures in between square-planar and tetrahedral fall within the range of 0 to 1.[36] Both measures of distortion, listed in Table 3, are in good agreement and support the distortion from square-planar towards tetrahedral for **Cu-*R*-L1**, **Cu-*S*-L1** and **Cu-*R*-L2**.

Due to the non-planar coordination at the copper atom in the above complexes, the identical *N*^*O* ligands afford C_2-symmetrical metal complexes with metal-centered Λ- or Δ-chirality (*cf.* Scheme 1). The absolute configuration Δ or Λ at the copper atom is determined by considering the screw orientation of the chelate ring planes around the pseudo-C_2 axis passing through the copper atom (Scheme 1). For the given (*R*) ligand chirality only the Λ-configuration can be found for **Cu-*R*-L1** as based on the absolute structure or Flack parameter of 0.042(2) or less for two crystals from different batches (*cf.* Table 5 in the Experimental Section).[25] This Flack parameter close to zero confirms the correct absolute structure and, together with other refinement parameters, normal atom temperature factors and the absence of molecular disorder, excludes that any significant amount of complexes with the opposite metal chirality is present within the investigated crystal. Conversely two crystals from a batch of **Cu-*S*-L1** only showed the Δ-configuration at the copper atom with Flack parameters[25] of 0.07(4) or less (Fig. 2, Table 5). We view this as sufficient evidence for the formation of enantiopure crystals and against a diastereomeric conglomerate, that is, the formation of both **Δ-Cu-*R*-L1** and **Λ-Cu-*R*-L1** in a crystal batch with Δ- and Λ-configuration crystallizing in separate crystals, akin to spontaneous resolution.[16b,39]

In compound **Cu-*R*-L2** both Δ- and Λ-configurations are present as two symmetry-independent molecules in the asymmetric unit (confirmed by measuring two crystals from the same batch). Hence, crystals of **Λ/Δ-Cu-*R*-L2** are diastereomeric such that two diastereomers are present in equal amounts in a well-defined arrangement within the lattice of a homogeneous crystalline compound.

We note that the molecular structure of **Cu-*R*-L1** as a dichloromethane solvate[33a,34] has been reported in the slightly different non-centrosymmetric space group $P2_12_12_1$ instead of $P2_12_12$ for the solvent-free structure reported here. Also, in that report no attention was given to the Λ/Δ-configuration at the copper atom and the formation of **Λ-Cu-*R*-L1**.

The question arises whether the difference in the formation of enantiopure *versus* diastereomeric crystals for complexes of **L1** and **L2** and the small degree of distortion at Cu for **L4** can be due to the inter-molecular interactions in the solid-state packing or whether they arise from intra-molecular interactions. Analysis of the packing diagrams (Fig. 5) does not give any indication that only an enantiopure packing or a diastereomeric packing should have been possible.

The packing differs as a consequence of the different ligand and space group. Yet, no significant π···π or only some C–H···π interactions[40] are found by PLATON[41] as inter-molecular

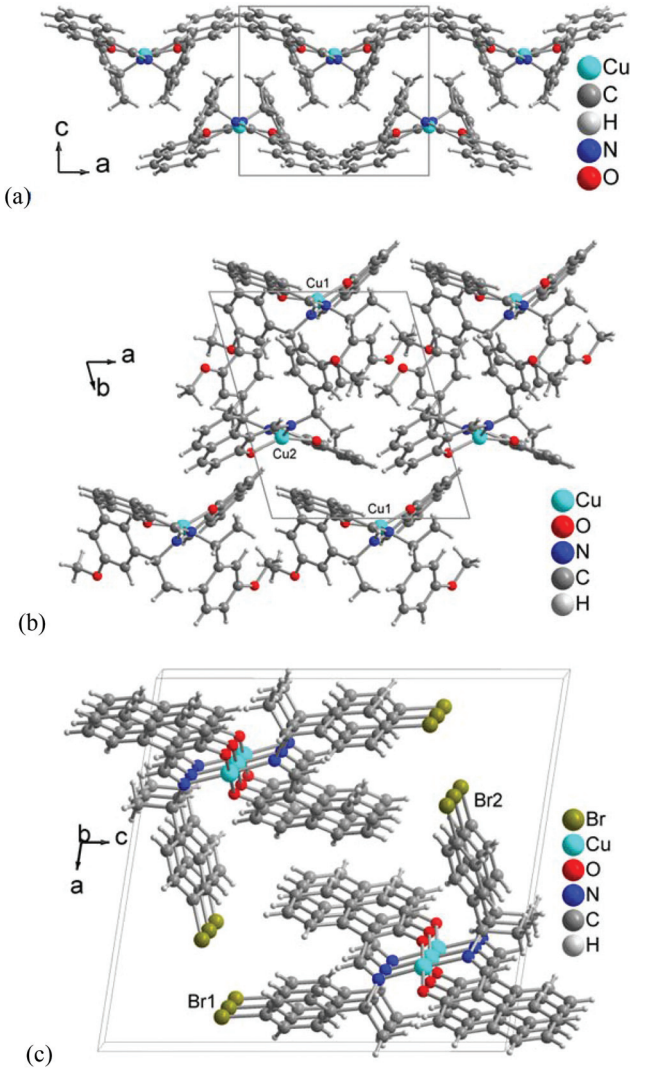

Fig. 5 Sections of the packing diagrams for (a) **Λ-Cu-*R*-L1**, (b) **Λ/Δ-Cu-*R*-L2** and (c) **Λ-Cu-*R*-L4**. See Fig. S2 in ESI† for additional views of the packing diagrams.

interactions to rationalize the formation of enantiopure *versus* diastereomeric crystals. The analysis of short ring-interactions for possible π-stacking interactions yielded rather long centroid–centroid distances (>4.0 Å) together with non-parallel ring planes and large slip angles (β, γ > 30°) (see ESI†). In comparison, significant π-stackings show rather short centroid–centroid contacts (<3.8 Å), near parallel ring planes, small slip angles (β, γ < 25°) and vertical displacements (slippage < 1.5 Å) which translate into a sizable overlap of the aryl-plane areas.[40] Significant intermolecular C–H···π contacts start around 2.7 Å for the (C–)H···ring centroid distances with C–H···centroid angle > 145°. In the packing of **Λ/Δ-Cu-*R*-L2** and **Λ-Cu-*R*-L4** two C–H···π contacts each approach the criteria for significant intermolecular C–H···π contacts. Other than that, there are no strong classical hydrogen-bonding interactions which could organize enantiomers in cases of spontaneous resolution.[16b,39c] From a visual inspection it cannot be rationalized why, for example, the Λ-configuration of **Cu-*R*-L1** should not

be able to pack with the Δ-configuration or why **Cu-*R*-L2** packs with both metal configurations. In the structure of **Λ-Cu-*R*-L4** the Br···Br contacts of 3.673(3) Å are in the range discussed for such soft–soft contacts.[42]

In the structures of **Cu-L1** the co-presence of the two diastereomers might even lead to an improved packing coefficient. The packing coefficients for the majority of crystals are between 0.65 and 0.77 as for the close-packing of spheres and ellipsoids.[43] Noteworthy, the packing coefficient of **Λ-Cu-*R*-L1** and **Δ-Cu-*S*-L1** is smaller than 0.65 and there is surplus "empty space" on the order of 2.1–5.6% (depending on temperature, see ESI†). In **Λ/Δ-Cu-*R*-L2** and **Λ-Cu-*R*-L4** the packing coefficients are between 0.66 and 0.69 with no potential solvent void (see ESI†).

All **Cu-L** compounds presented here have in principle a two-fold symmetry. However, crystallographically the two-fold molecular symmetry is retained in the solid state only in **Λ-Cu-*R*-L1** and **Δ-Cu-*S*-L1** where the Cu atom sits on a special position with the 2_1 axis passing through the molecule. In **Λ/Δ-Cu-*R*-L2** and **Λ-Cu-*R*-L4** the non-symmetric orientation of the $-C_6H_4OMe$ and $-C_6H_4Br$ groups, respectively, in the solid state (see Fig. 3 and 4) does not coincide with two-fold crystal symmetry. Perhaps, in order to achieve a closer packing, the **Cu-L1** molecules would have to give up their two-fold molecular symmetry upon crystallization.

From the absence of decisive inter-molecular interactions in the solid-state packing we suggest that intra-molecular interactions already lead to the preferential formation of one diastereomer in solution (see below). Then rather small packing forces and differences can either give enantiopure or diastereomeric crystals through the chemical equilibrium between Λ- and Δ-configuration. To further support the molecular origin of diastereoselectivity in, *e.g.*, **Cu-*R*-L1** we carried out chiroptical spectroscopic studies in solution using circular dichroism (CD).

UV-vis absorption and CD spectra

The use of electronic (CD) or vibrational circular dichroism (VCD) has allowed in the past the assignment of the stereochemistry of several tetrahedral or pseudo-tetrahedral metal complexes with Schiff-base ligands.[6c,d,7c,d,19,21,22,34]

UV-vis absorption and CD spectra measured in solution for all the complexes considered are shown in Fig. 6–9. Absorption spectra show consistent similarities over the whole measured spectral range. In the visible region there is a weak and broad band around 650 nm, due to the superposition of several metal-centred transitions typical of the Cu(II) core.[7a–e] The next bands in the UV region are specific of the ligand considered, and are allied to ligand-to-metal charge transfer or intra-ligand transitions.

The electronic CD spectra of all enantiomeric couples, that is, **Cu-*R*-L1/Cu-*S*-L1**, **Cu-*R*-L3/Cu-*S*-L3**, and **Cu-*R*-L4/Cu-*S*-L4**, show the expected mirror–image relationship (Fig. 6–9) in cyclohexane. Although the CD spectra show some variation along the series, several consistent features may also be observed similarly to absorption spectra. In fact, the complexes **Cu-*R*-L1**, **Cu-*R*-L2**, **Cu-*R*-L3** and **Cu-*R*-L4** are characterized by the following series of CD bands indicative of *R* ligand configuration (band wavelength, sign and strength are indicated): *ca.* 700 (–, weak); *ca.* 600 (+, weak); *ca.* 400 (+, medium); *ca.* 315 nm (–, medium); *ca.* 260 (–, strong); *ca.* 220 (+, strong). Other bands depend more on the ligand nature and are not conserved along the series.

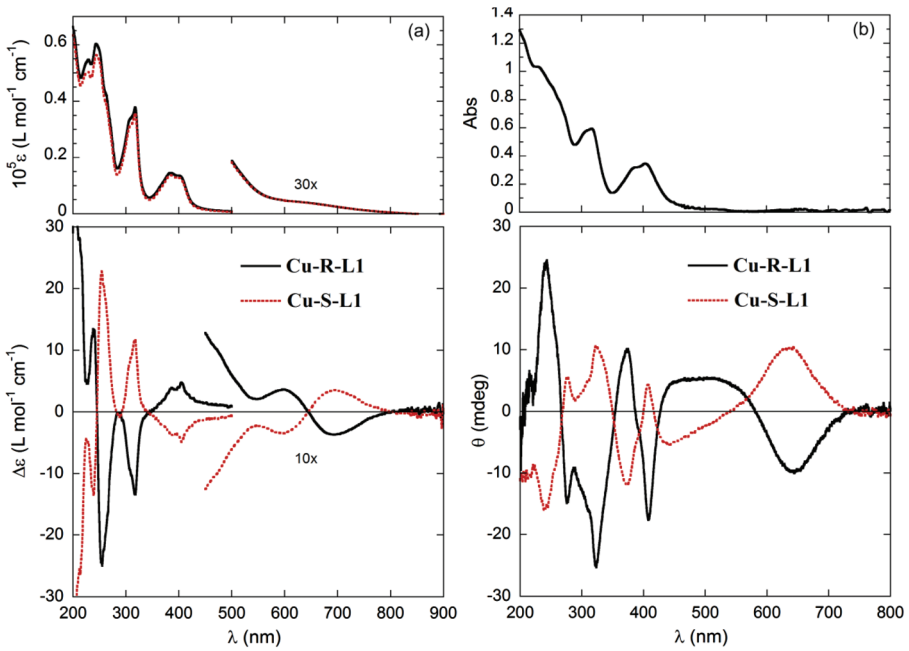

Fig. 6 (a) UV-vis and CD spectra of **Cu-*R*-L1** and **Cu-*S*-L1** in cyclohexane (2.13 and 2.23 mM, respectively); cell path-length: 0.1 mm, 200–500 nm; 5 mm, 425–600 nm; 10 mm, 400–900 nm. (b) UV-vis and CD spectra of **Cu-*R*-L1** and **Cu-*S*-L1** in the solid state as KCl pellets.

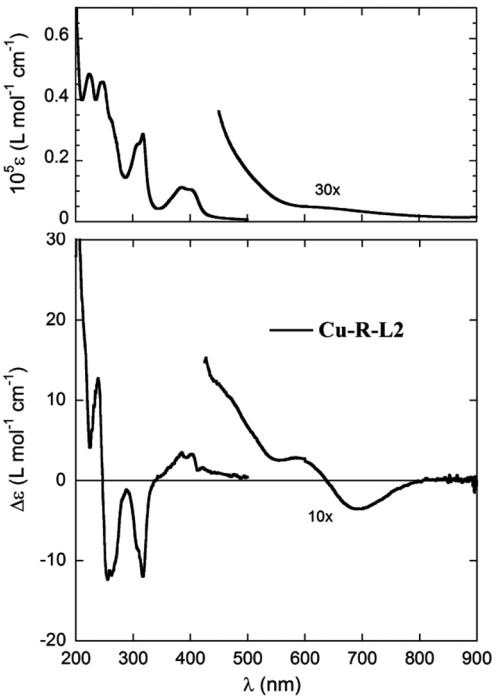

Fig. 7 UV-vis and CD spectra of **Cu-*R*-L2** in cyclohexane (2.53 mM); cell path-length: 0.1 mm, 200–500 nm; 5 mm, 425–600 nm; 10 mm, 400–900 nm.

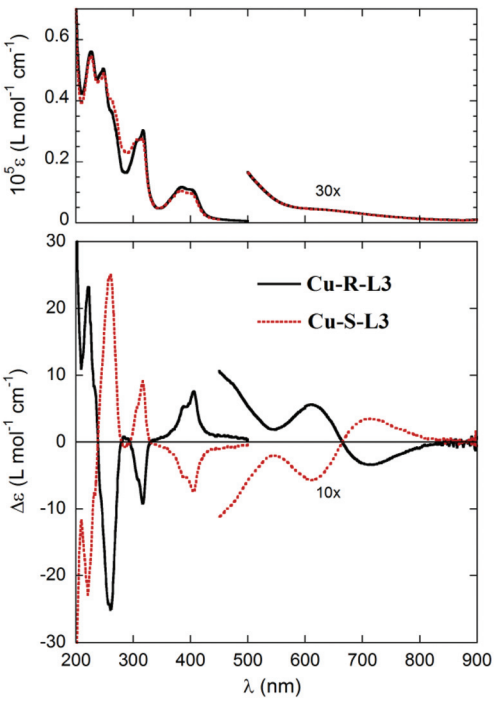

Fig. 8 UV-vis and CD spectra of **Cu-*R*-L3** and **Cu-*S*-L3** in cyclohexane (2.21 and 2.32 mM, respectively); cell path-length: 0.1 mm, 200–500 nm; 5 mm, 425–600 nm; 10 mm, 400–900 nm.

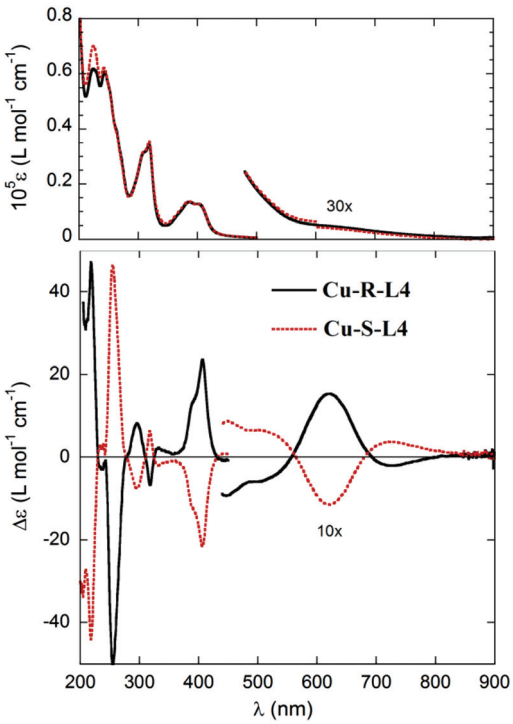

Fig. 9 UV-vis and CD spectra of **Cu-*R*-L4** and **Cu-*S*-L4** in cyclohexane (1.95 and 1.90 mM, respectively); cell path-length: 0.1 mm, 200–500 nm; 5 mm, 425–600 nm; 10 mm, 400–900 nm.

For the crystalline complexes **Cu-*R*-L1** and **Cu-*S*-L1**, solid-state CD spectra[44] were also recorded (Fig. 6b). The sequence of bands is similar to the solution spectra in the visible range, while major differences emerge in the UV region. In particular, some of the bands are strongly altered or reversed in sign in the solid state with respect to the solution. In the following section we interpret the source of such discrepancies. For the crystalline complex **Cu-*R*-L2**, on the contrary, no reproducible solid-state CD spectrum could be obtained.

It is interesting to compare the solution and solid-state CD spectra of **Cu-*R*-L1** in terms of *g*-factor, that is, the wavelength-dependent ratio between the absorption and the CD spectrum $g = \Delta\varepsilon/\varepsilon = \Delta A/A$ (A is the absorbance and ΔA the differential absorbance) (Fig. 6a and b). In the UV region, where absorption maxima are more easily identified, the range of *g*-factor values is 2–3 × 10^{-4} in the solution spectrum and 2–4 × 10^{-4} in the solid-state spectrum. Even correcting the latter for the scattering effects on the baseline, the *g*-factor attains at most a value of $\approx 10^{-3}$.

Geometry optimizations and CD calculations

A thorough computational procedure was carried out with the aim to rationalize the observed UV-vis/CD spectra and allow the assignment of the preferential **Λ** or **Δ** chirality assumed by the metal centre. Time-dependent density functional theory (TDDFT) is currently recognized as one of the methods with the best cost/efficiency compromise to simulate the UV-vis and

CD spectra of medium-size transition metal complexes.[45,46] When open-shell metal complexes are involved, as in the present case, TDDFT may suffer from various pitfalls, in particular spin contamination.[47] Our results demonstrate that the use of properly chosen calculation conditions may reproduce very satisfactorily both the structure and the CD spectra of the Cu(II) complexes under investigation. In particular, we employed M06 functional, which is especially well-suited for metal complexes.[48]

The compound considered in the calculations was **Cu-*R*-L1**, taken as a model for the whole series. Starting from the X-ray structure, a conformational search was run to investigate the conformational space associated with the ligand flexibility, using the Molecular Merck force field (MMFF). All MMFF structures obtained were re-optimized with DFT at the B3LYP/6-31G(d) level, leading to a first set of structures with **Λ-Cu-*R*-L1** configuration. The same procedure was followed for a structure with opposite configuration at the metal but the same ligand configuration, **Δ-Cu-*R*-L1**. The two sets of structures are composed each of 2 conformers only, with Boltzmann populations above 2% at 300 K accounting in both cases for 97% overall population. The structures, relative energies and populations are reported in Fig. 10 and 11. Higher energy structures had relative internal energies above 2.2–2.5 kcal mol^{-1} with respect to the respective lowest energy minimum, and negligible Boltzmann populations at 300 K. According to DFT calculations, the **Λ-Cu-*R*-L1** diastereomer is more stable than the **Δ-Cu-*R*-L1** diastereomer by at least 0.64 kcal mol^{-1} (considering the lowest energy conformers in both cases). The theoretical **Λ : Δ** diastereomeric ratio is 77 : 23, and the diastereomeric excess (*i.e.*, the (**Λ** − **Δ**)/(**Λ** + **Δ**) ratio) is 54%. It is interesting to compare the lowest-energy DFT-optimized structure having **Λ**-Cu-*R* configuration shown in Fig. 10 with the X-ray structure determined for the **Cu-*R*-L1** complex (also having **Λ** configuration) shown in Fig. 2, which served as the starting structure for the calculations. The conformation of the chiral amine moieties is very similar in the two cases. As a consequence of the optimization, however, the distortion from the square-planar geometry is increased. In fact, the θ dihedral angle defined in Scheme 4 is 40.7° for the DFT geometry,

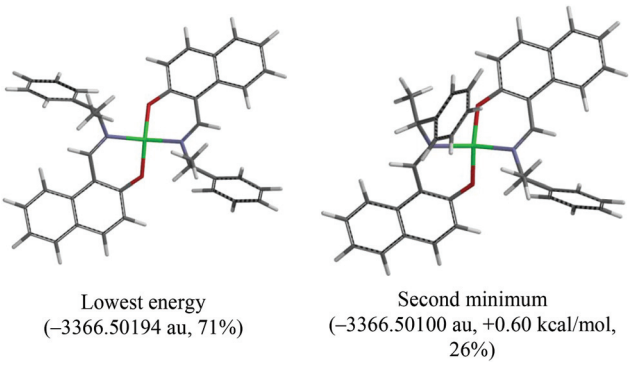

Fig. 10 B3LYP/6-31G(d) structures of the **Λ-Cu-*R*-L1** complex.

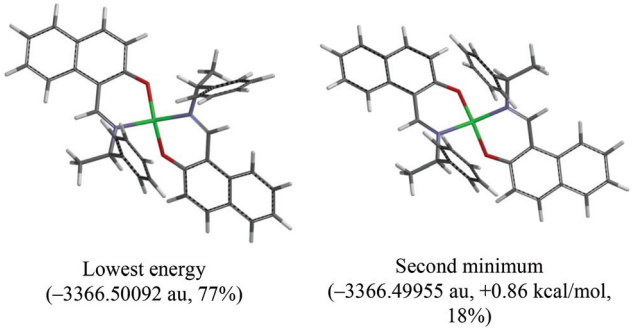

Fig. 11 B3LYP/6-31G(d) structures of the **Δ-Cu-*R*-L1** complex.

which leads to a $\tau_{\text{tet-sq}}$ index of 0.45; correspondingly, the τ_4 index amounts to 0.45 too.

CD calculations were run with the TDDFT method using the M06/TZVP combination after a preliminary screening of various DFT functionals and basis sets. M06/TZVP calculations were run on B3LYP/6-31G(d) optimized structures of both **Λ-Cu-*R*-L1** and **Δ-Cu-*R*-L1** complexes, considering two low-energy minima in both cases; the resulting spectra are reported in the ESI.† In Fig. 12 we depict the calculated Boltzmann-weighted averages at 300 K.

The main observations following the calculations are: (a) the calculated UV-vis absorption spectra are very similar for the four structures; (b) the calculated CD spectra for the two minima of each diastereomer are similar, except for a small wavelength shift; (c) the calculated average CD spectra for the two diastereomers with opposite configuration at the metal centre [Λ-Cu-*R* and Δ-Cu-*R*] are almost mirror images (Fig. 12). It may be inferred that the calculated CD spectra are largely dominated by the overall nature of the complex, and in particular are determined by the configuration at the metal centre (Λ *vs.* Δ). In contrast, they are only slightly affected by the conformation assumed by the chiral moiety and its absolute configuration [(*R*,*R*) or (*S*,*S*)]. The agreement between the experimental CD spectrum of **Cu-*R*-L1** (Fig. 6a) and that calculated for the **Λ-Cu-*R*-L1** configuration (Fig. 12, left) is very good in the whole significant range (above 300 nm of the calculated spectrum), apart from a wavelength shift seen especially in the UV region. The first five major bands appearing in the experimental CD spectrum are all reproduced by the calculations. It may be therefore concluded that electronic CD spectroscopy is entirely able to establish the Λ or Δ chirality of the Schiff-base complexes considered here. In particular, we demonstrated that the following relationship holds for the complexes under analysis:

(*R*) ligand configuration ⇔ dominant Λ chirality
(*S*) ligand configuration ⇔ dominant Δ chirality

Concerning the solid state, it is interesting to note that the CD spectrum calculated on the X-ray structure determined for **Λ-Cu-*R*-L1** (see ESI†) is very similar both in shape and intensity to the Boltzmann average CD shown in Fig. 12 (left). This finding suggests that the differences observed between the

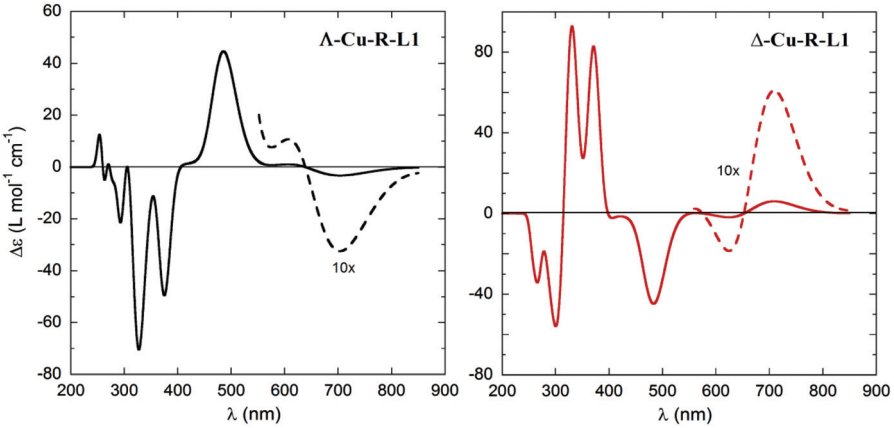

Fig. 12 CD spectra calculated at the M06/TZVP//B3LYP/6-31G(d) level for the two diastereomers **Λ-Cu-*R*-L1** (left) and **Δ-Cu-*R*-L1** (right), as Boltzmann averages at 300 K of the spectra (two in each case) calculated for the low-energy minima shown in Fig. 10 and 11. Gaussian band shape with exponential bandwidth σ = 0.15 eV.

experimental solution and solid-state CD spectra of **Cu-*R*-L1** are not due to a conformational rearrangement, but are related to intermolecular couplings in the crystals.[49] The comparison between the calculated spectra for **Λ-Cu-*R*-L1** and **Δ-Cu-*R*-L1** on DFT geometries, and for **Λ-Cu-*R*-L1** on the X-ray geometry, has also some implications on the estimation of the diastereomeric excess. Since the calculated spectra for **Λ-Cu-*R*-L1** and **Δ-Cu-*R*-L1** are almost mirror images, the *g*-factor of the experimental spectra may be considered roughly proportional to the diastereomeric excess in solution. In the X-ray structure of **Cu-*R*-L1**, only the **Λ** form is observed. Based on the observations made above for the *g*-factor measured on experimental solution and solid-state CD spectra, we may conclude that the diastereomeric excess in solution is large, above 50% and possibly reaching 100% for **Cu-*R*-L1** in favor of the **Λ-Cu-*R*-L1** complex. We also observe that the lower limit is in accord with DFT calculations discussed above. Although the estimated value for the diastereomeric excess in solution cannot be entirely transferred to the complexes of the remaining ligands **L2–L4**, the consistent intensities seen for the diagnostic bands in the experimental CD spectra (Fig. 6–9) point to a substantially similar behavior. In particular, the results for compound **Cu-*R*-L2** demonstrate that, upon dissolving the diastereomeric crystals of **Λ/Δ-Cu-*R*-L2**, equilibration occurs in solution again in favor of the **Λ-Cu-*R*-L2** complex.

A straightforward assignment of the calculated CD spectra is hampered by the complexity of the system and the large number of transitions. A list of transitions with non-negligible oscillator and/or rotational strengths calculated for the lowest energy structure of the **Λ-Cu-*R*-L1** complex at the M06/TZVP//B3LYP/6-31G(d) level is reported in the ESI†. In Table 4 we report a simplified assignment of only the relevant transitions, *i.e.* those most contributing to the observed UV-vis and CD spectra. It must be stressed that, as it appears clearly from the ESI,† every transition derives from many single excitations. Thus, the assignment reported in Table 4, based on orbital and population analysis, is very simplified. The most important conclusion to be drawn is the absence of a clear separation between metal-centered and ligand-centered transitions, because several metal-centered transitions occur deeply in the UV region of the spectrum. Therefore any spectral assignment in terms of simple M–M, L–M or L–L transitions (metal d–d, ligand-to-metal, and ligand-only transitions) must be considered a heavy and somewhat arbitrary approximation for most observed bands.

Table 4 Main transitions calculated for the lowest-energy structure of the **Λ-Cu-R-L1** complex with M06/TZVP//B3LYP/6-31G(d), contribution to the major observed CD bands, and simplified assignment

Exc. state	Calculated transition wavelength (nm)	Observed CD band (maximum wavelength, nm, and sign)	Assignment [a]	Notes[a]
2	678	692 (−)	M–M	
3	639	597 (+)	M–M, L–M	
4	624		M–M, L–M, CT	
8	482	*ca.* 400 (+)	M–M, L–M	Localized on Np
11	379	317 (−)	L–M	Localized on Np
12	378		L–M	Localized on Np
13	373		L–L	π–π* on Np, short-axis
14	368		L–L	π–π* on Np, short-axis
23	329	252 (−)	L–L	π–π* and n–π* on Np
24	327		L–M	Localized on Ph and Np

[a] M–M, metal d–d; L–M, ligand-to-metal; L–L, ligand-only transitions; CT, charge transfer; Np, 2-hydroxy-1-naphthaleneiminato; Ph, phenyl.

Conclusions

Enantiopure *N*,*O*-chelate Schiff-base ligands (*R* or *S*)-*N*-1-(Ar)-ethyl-2-oxo-1-naphthaldimine (Ar = C_6H_5, *m*-C_6H_4OMe,

p-C_6H_4OMe, and *p*-C_6H_4Br) induce metal-centered Λ/Δ-chirality in distorted square-planar $Cu(N^\wedge O)_2$ complexes. In most cases, the *R*- or S-ligand diastereoselectively induces a Λ- or Δ-Cu configuration, respectively, in the solid state. Only in one case, the *N*^*O*-ligand with *m*-C_6H_4OMe combines both the Λ- and Δ-Cu configurations as a diastereomeric pair in the crystal packing. In solution, a diastereomeric excess towards Λ-Cu or Δ-Cu configuration is found for *R*- or *S*-ligand, respectively, as evidenced by CD spectra. A TDDFT calculation of CD spectra for the diastereomeric pair Λ- and Δ-Cu-*R* suggests that the spectra are largely dominated by the configuration at the metal center (Λ *vs.* Δ). Cyclic voltammetry measurements reveal a quasi-reversible redox wave relating to one-electron transfer for the $[Cu^{II}L_2]^0/[Cu^{I}L_2]^{-1}$ couple. DSC analyses correspond to a phase transformation of the complexes from distorted square-planar/tetrahedral to regular tetrahedral showing an exothermic peak between 377 and 478 K.

Our results demonstrate that the metal chirality of a distorted square-planer complex may be efficiently controlled by the ligand chirality. Although the stereochemical control may occur in both solution and solid state, the extent of the two phenomena varies from ligand to ligand. Thus, a different behavior in the two states may be tuned by modifying the ligand skeleton by introducing different substituents on the aromatic ring.

Experimental section

IR-spectra were recorded on a Nicolet iS10 spectrometer as KBr discs at ambient temperature. UV-vis spectra were obtained using a Shimadzu UV 1800 spectrophotometer in cyclohexane at 25 °C. Elemental analyses were done on a Vario EL instrument from Elementaranalysensysteme. Thermal analysis was performed on a SHIMADZU DSC-60 differential scanning calorimeter (DSC), in a heating range of 303–553 K and at a rate of 10 K min^{-1}. An Epsilon™ Instruments (BASi) electrochemical analyzer was used for cyclic voltammetry (CV) experiments in acetonitrile containing tetra-*N*-butyl-ammonium-hexafluorophosphate (TBAP) as a supporting electrolyte. The three-electrode measurement was carried out at 298 K with a platinum disc working electrode, a platinum wire auxiliary electrode and a Ag/AgCl reference electrode. The solution containing the copper(II) complex and TBAP was deoxygenated for 15 minutes with nitrogen gas. Polarimetric measurements were carried with a UniPol L instrument in $CHCl_3$ at 25 °C. CD spectra were obtained using a JASCO Spectropolarimeter (J715) in cyclohexane on 2–2.5 mM samples. For each solution sample, three distinct spectra were recorded using cells with different path-lengths (0.1 mm, 5 mm and 10 mm) to cover the whole spectral range from 190–200 to 900 nm by keeping the absorbance below 1.5 AU. Solid-state samples for CD were prepared by mixing 1–2 small crystals with approximately 100 mg of oven-dried KCl, then pressing the disc at 10 tons for about 15 min. The resulting disc was checked for homogeneity and transparency. Several discs were prepared for each compound. For each disc, four different spectra were recorded by rotating the disc around the incident light direction and by flipping the disc with respect to the vertical, to check the presence of artifacts. ^{1}H-NMR spectra were recorded on a Bruker Avance DPX 200 spectrometer operating at 200 MHz (^{1}H) at 20 °C with calibration against the residual protonated solvent signal ($CDCl_3$ ^{1}H-NMR, 7.25 ppm). EI-MS: Thermo-Finnigan TSQ 700. Isotopic distributions for $^{63/65}$Cu and $^{63/65}$Cu + $^{79/81}$Br containing ions are clearly visible in the mass spectra. The syntheses of enantiopure Schiff bases, (*R* or *S*)-*N*-1-(Ar)ethyl-2-oxo-1-naphthaldimine, have been described in our previous report.[16a,c]

General procedure to synthesise the complexes

Two equivalents of enantiopure (*R* or *S*)-*N*-1-(phenyl)ethyl-2-oxo-1-naphthaldimine (*R*- or *S*-**HL1**) (760 mg, 2.76 mmol) dissolved in 5 mL of methanol was added into 10 mL of a hot methanolic solution of $Cu(O_2CCH_3)_2{\cdot}H_2O$ (276 mg, 1.38 mmol) and the solution was stirred for about 5–6 h at room temperature. The color changes from light green to brown. Then the solvent was reduced to ~50% *in vacuo*, and this solution was allowed to stand for crystallization *via* slow solvent evaporation at rt. Dark brown crystals of **Cu-*R*-L1** (data set CuR12), suitable for X-ray measurements, were obtained within 5–6 d from methanol. The crystals were separated, washed three times with methanol and dried in air for 2–3 d. The same procedure was followed for using the Schiff bases (*R* or *S*)-*N*-1-(Ar)ethyl-2-oxo-1-naphthaldimine {Ar = *m*-$OMeC_6H_4$ (**HL2**), *p*-$OMeC_6H_4$ (**HL3**), and *p*-BrC_6H_4 (**HL4**)}, respectively. Single crystals of X-ray quality for **Cu-*R*-L1** (data set CuRL1a), **Cu-*S*-L1** (CuSL1-II or CuSL1-III), and **Cu-*R*-L4** were grown by layer-diffusion of methanol into concentrated complex solution in $CHCl_3$ or by layer-diffusion of ethanol into concentrated complex solution in CH_2Cl_2–$CHCl_3$ (50%, v/v). Crystals of **Cu-*R*-L2** (CuR14a or CuRL2-LT) were obtained following the same procedure as that for CuR12.

Bis[{(*R*)-*N*-(phenyl)ethyl-2-oxo-1-naphthaldiminato-κ^2*N*,*O*}]-copper(II) (Cu-*R*-L1). Yield 700 mg (83%). $[\alpha]_D$: +75.6° (*c* = 0.33 g/100 mL, $CHCl_3$ at 25 °C). IR (KBr, cm^{-1}): ν = 3051, 2976, 2927w (H–C), 1616vs (C═N), and 1540 s (C═C). EI-MS (70 eV): *m*/*z* (%) = 611 (70) $[M]^+$, 336 (50) $[M - HL1]^+$, 275 (100) $[HL1]^+$, 234 (35) $[C_{10}H_6(O)(CHNH)Cu + H]^+$, 170 (45) $[C_{10}H_6(O)(CHNH)]^+$, and 105 (80) $[C_6H_5CHCH_3]^+$. APCI-MS (pos.): *m*/*z* (%) = 950 (20) $[M_2 - L1 + H_2]^+$, 948 (20) $[M_2 - L1]^+$, 612 (100) $[M + H]^+$, 369 (20) $[M - L1 + CH_3OH]^+$, 337 (5) $[M - L1]^+$, and 274 (15) $[HL1 - H]^+$. ^{1}H NMR (200 MHz, KCN/dmso-d6): δ = 1.50 (d, J_{HH} = 6.6 Hz, 3H, C*H*$_3$), 4.34 (q, J_{HH} = 6.6 Hz, 1H, C*H*), 6.55 (d, J_{HH} = 9.1 Hz, 1H, H_{Ar}), 6.82 (t, J_{HH} = 6.9, 7.5 Hz, 1H, H_{Ar}), 7.17 (dt, J_{HH} = 7.1, 6.9 Hz, J_{HH} = 1.2 Hz, 3H, H_{Ar}), 7.29–7.38 (m, 4H, H_{Ar}), 7.44 (d, J_{HH} = 8.8 Hz, 1H, H_{Ar}), 9.20 (s, 1H, C*H*N), and 9.46 (d, J_{HH} = 8.5 Hz, 1H, H_{Ar}). $C_{38}H_{32}N_2O_2Cu$ (612.23): calcd C 74.55, H 5.27, N 4.58; found C 73.04, H 5.51, N 4.38%.

Bis[{(*S*)-*N*-(phenyl)ethyl-2-oxo-1-naphthaldiminato-κ^2*N*,*O*}]-copper(II) (Cu-*S*-L1). Yield 650 mg (77%). $[\alpha]_D$: −74.6° (*c* = 0.42 g/100 mL, $CHCl_3$ at 25 °C). IR (KBr, cm^{-1}): ν = 3055, 2981,

2928w (H–C), 1615vs (C═N), and 1541 s (C═C). EI-MS (70 eV): *m/z* (%) = 611 (60) $[M]^+$, 336 (55) $[M - HL1]^+$, 275 (100) $[HL1]^+$, 234 (45) $[C_{10}H_6(O)(CHNH)Cu + H]^+$, 170 (450) $[C_{10}H_6(O)(CHNH)]^+$, and 105 (70) $[C_6H_5CHCH_3]^+$. $C_{38}H_{32}N_2O_2Cu$ (612.23): calcd C 74.55, H 5.27, N 4.58; found C 73.54, H 5.41, N 4.30%.

Bis[{(*R*)-*N*-(3-methoxphenyl)ethyl-2-oxo-1-naphthaldiminato-κ²*N*,*O*}]copper(II) (Cu-*R*-L2). Yield 765 mg (82%). $[\alpha]_D$: −78.0° (*c* = 0.90 g/100 mL, $CHCl_3$ at 25 °C). IR (KBr, cm^{-1}): ν = 3051, 2961, 2933w (H–C), 1616, 1605vs (C═N), and 1541 s (C═C). EI-MS (70 eV): *m/z* (%) = 671 (65) $[M]^+$, 366 (60) $[M - HL2]^+$, 305 (100) $[HL2]^+$, 234 (50) $[C_{10}H_6(O)(CHNH)Cu + H]^+$, 170 (30) $[C_{10}H_6(O)(CHNH)]^+$, 135 (80) $[C_6H_4(OCH_3)CHCH_3]^+$, 105 (17) $[C_6H_5CHCH_3]^+$. APCI-MS (pos.): *m/z* (%) = 1040 (15) $[M_2 - L2 + H_2]^+$, 1038 (15) $[M_2 - L2]^+$, 672 (100) $[M + H]^+$, 399 (20) $[M - L2 + CH_3OH]^+$, and 304 (5) $[HL2 - H]^+$. ^{1}H NMR (200 MHz, KCN/dmso-d_6): δ = 1.48 (d, J_{HH} = 6.6 Hz, 3H, C*H*$_3$), 3.75 (s, 3H, OC*H*$_3$), 4.31 (q, J_{HH} = 6.5 Hz, 1H, C*H*), 6.56 (d, J_{HH} = 9.1 Hz, 1H, H_{Ar}), 6.74–6.86 (m, 2H, H_{Ar}), 7.04 (d, J_{HH} = 7.3 Hz, 2H, H_{Ar}), 7.12–7.28 (m, 2H, H_{Ar}), 7.32–7.38 (m, 2H, H_{Ar}), 9.18 (s, 1H, C*H*N), and 9.46 (d, J_{HH} = 8.4 Hz, 1H, H_{Ar}). $C_{40}H_{36}N_2O_4Cu$ (672.28): calcd C 71.46, H 5.40, N 4.17; found C 70.91, H 5.30, N 4.01%.

Bis[{(*R*)-*N*-(4-methoxphenyl)ethyl-2-oxo-1-naphthaldiminato-κ²*N*,*O*}]copper(II) (Cu-*R*-L3). Yield 750 mg (81%). IR (KBr, cm^{-1}): ν = 3050, 2972, 2929w (H–C), 1616, 1605vs (C═N), and 1541 s (C═C). EI-MS (70 eV): *m/z* (%) = 671 (60) $[M]^+$, 366 (65) $[M - HL3]^+$, 305 (100) $[HL3]^+$, 234 (35) $[C_{10}H_6(O)(CHNH)Cu + H]^+$, 170 (10) $[C_{10}H_6(O)(CHNH)]^+$, 135 (85) $[C_6H_4(OCH_3)CHCH_3]^+$, and 105 (20) $[C_6H_5CHCH_3]^+$. APCI-MS (pos.): *m/z* (%) = 1040 (20) $[M_2 - L3 + H_2]^+$, 1038 (18) $[M_2 - L3]^+$, 672 (100) $[M + H]^+$, 399 (10) $[M - L3 + CH_3OH]^+$, and 304 (10) $[HL3 - H]^+$. $C_{40}H_{36}N_2O_4Cu$ (672.28): calcd C 71.46, H 5.40, N 4.17; found C 70.38, H 5.43, N 3.91%.

Bis[{(*S*)-*N*-(4-methoxphenyl)ethyl-2-oxo-1-naphthaldiminato-κ²*N*,*O*}]copper(II) (Cu-*S*-L3). Yield 720 mg (78%). IR (KBr, cm^{-1}): ν = 3050, 2974, 2927w (H–C), 1616, 1605vs (C═N), and 1541s (C═C). EI-MS (70 eV): *m/z* (%) = 671 (50) $[M]^+$, 366 (45) $[M - HL3]^+$, 305 (100) $[HL3]^+$, 234 (25) $[C_{10}H_6(O)(CHNH)Cu + H]^+$, 170 (15) $[C_{10}H_6(O)(CHNH)]^+$, 135 (75) $[C_6H_4(OCH_3)CHCH_3]^+$, and 105 (30) $[C_6H_5CHCH_3]^+$. $C_{40}H_{36}N_2O_4Cu$ (672.28): calcd C 71.46, H 5.40, N 4.17; found C 72.10, H 5.22, N 3.99%.

Bis[{(*R*)-*N*-(4-bromophenyl)ethyl-2-oxo-1-naphthaldiminato-κ²*N*,*O*}]copper(II) (Cu-*R*-L4). Yield 850 mg (80%). IR (KBr, cm^{-1}): ν = 3058, 2971, 2928w (H–C), 1616, 1608vs (C═N), and 1541s (C═C). EI-MS (70 eV): *m/z* (%) = 767 (10) $[M]^+$, 414 (20) $[M - HL4]^+$, 353 (15) $[HL4]^+$, 305 (100) $[(C_6H_5CHCH_3NH_2)_2Cu]^+$, 234 (40) $[C_{10}H_6(O)(CHNH)Cu + H]^+$, 183 (15) $[C_6H_4(Br)(CHCH_3)]^+$, 170 (40) $[C_{10}H_6(O)(CHNH)]^+$, 135 (25) $[C_6H_5CHCH_3(NHCH_3)]^+$, and 104 (25) $[CH_3CHC_6H_5 - H]^+$ (isotopic distribution patterns for ($^{63/65}$Cu + $^{79/81}$Br) containing ions are visible following the peaks at 767 and 414 and those for $^{79/81}$Br containing ions at 353 and 183). APCI-MS (pos.): *m/z* (%) = 1184 (20) $[M_2 - L4 + H_2]^+$, 770 (100) $[M + H_2 + H]^+$, 768 (45) $[M + H]^+$, and 354 (20) $[HL4 + H]^+$. ^{1}H NMR (200 MHz, KCN/dmso-d_6): δ = 1.48 (d, J_{HH} = 6.5 Hz, 3H, C*H*$_3$), 4.32 (q, J_{HH} = 6.6 Hz, 1H, C*H*), 6.54 (d, J_{HH} = 9.1 Hz, 1H, H_{Ar}), 6.82 (dt, J_{HH} = 7.2 Hz, J_{HH} = 1.3 Hz, 1H, H_{Ar}), 7.36 (ddd, J_{HH} = 8.4, 6.8, J_{HH} = 1.4 Hz, 2H, H_{Ar}), 7.31–7.38 (m, 2H, H_{Ar}), 7.41–7.54 (m, 4H, H_{Ar}), 9.18 (s, 1H, C*H*N), and 9.42 (d, J_{HH} = 8.3 Hz, 1H, H_{Ar}). $C_{38}H_{30}N_2O_2Br_2Cu$ (770.02): calcd C 59.27, H 3.93, N 3.64; found C 59.10, H 4.04, N 3.49%.

Bis[{(*S*)-*N*-(4-bromophenyl)ethyl-2-oxo-1-naphthaldiminato-κ²*N*,*O*}]copper(II) (Cu-*S*-L4). Yield 875 mg (82%). IR (KBr, cm^{-1}): ν = 3055, 2974, 2927w (H–C), 1617, 1605vs (C═N), and 1541 s (C═C). – EI-MS (70 eV): *m/z* (%) = 767 (15) $[M]^+$, 414 (25) $[M - HL4]^+$, 353 (20) $[HL4]^+$, 305 (100) $[(C_6H_5CHCH_3NH_2)_2Cu]^+$, 234 (40) $[C_{10}H_6(O)(CHNH)Cu + H]^+$, 183 (25) $[C_6H_4(Br)(CHCH_3)]^+$, 170 (30) $[C_{10}H_6(O)(CHNH)]^+$, and 135 (20) $[C_6H_5CHCH_3(NHCH_3)]^+$ (isotopic distribution patterns for ($^{63/65}$Cu + $^{79/81}$Br) containing ions are visible following the peaks at 767 and 414 and those for $^{79/81}$Br containing ions at 353 and 183). $C_{38}H_{30}N_2O_2Br_2Cu$ (770.02): calcd C 59.27, H 3.93, N 3.64; found C 58.34, H 3.62, N 3.40%.

X-ray crystallography

Single-crystals of **Cu-*R*-L1**, **Cu-*S*-L1**, **Cu-*R*-L2** or **Cu-*R*-L4** were carefully selected under a polarizing microscope and mounted on a loop. *Data collection*: a Bruker APEX II CCD diffractometer with graphite-monochromated Mo-Kα radiation (λ = 0.71073 Å) at 203(2) K; ω-scans for the data sets CuR12 and CuR14a (see Tables 5 and 6). A Bruker Kappa APEX2 CCD diffractometer with a microfocus sealed tube, Mo-Kα radiation (λ = 0.71073 Å), a multi-layer mirror system, ω- and θ-scans for data sets (different crystals) of CuRL1a, CuSL1-II and -III, CuRL2-LT and CuRL4 (see Tables 5 and 6). Data collection and cell refinement using APEX2,[50] data reduction using SAINT (Bruker).[51] *Structure analysis and refinement*: the structures were solved by direct methods (SHELXS-97),[52] refinement was done by full-matrix least squares on F^2 using the SHELXL-97 program suite,[51] empirical (multi-scan) absorption correction using SADABS (Bruker).[53] All non-hydrogen positions were refined with anisotropic temperature factors. Hydrogen atoms for aromatic CH, aliphatic or olefinic CH, CH_2 and OH groups were positioned geometrically (C–H = 0.94 Å for aromatic CH, C–H = 0.94 Å for olefinic CH, 0.99 for aliphatic CH and 0.97 Å for CH_3) and refined using a riding model (AFIX 43 for aromatic CH, AFIX 13 for aliphatic CH, and AFIX 137 for CH_3), with $U_{iso}(H) = 1.2U_{eq}(CH, CH_2)$ and $U_{iso}(H) = 1.5U_{eq}(CH_3)$. Crystals of **Cu-*R*-L4** had a very thin needle shape which allowed only the collection of a lower quality data set. Details of the X-ray structure determinations and refinements are provided in Tables 5 and 6. Graphics were drawn using DIAMOND (Version 3.2).[38] Computations on the supramolecular interactions were carried out using PLATON for Windows.[41] The structural data for this paper have been deposited with the Cambridge Crystallographic Data Center (CCDC numbers 962481–962487).

Computational section

Conformational searches and geometry optimizations were run using Spartan'10 (Wavefunction, Inc., Irvine, CA). Excited-

Table 5 Crystal data and structure refinement for **Cu-L1**

Compound	**Λ-Cu-*R*-L1**	**Λ-Cu-*R*-L1**	**Δ-Cu-*S*-L1**	**Δ-Cu-*S*-L1**
Data set	CuR12	CuRL1a	CuSL1-II	CuSL1-III
Empirical formula	$C_{38}H_{32}CuN_2O_2$	$C_{38}H_{32}CuN_2O_2$	$C_{38}H_{32}CuN_2O_2$	$C_{38}H_{32}CuN_2O_2$
M/g mol^{-1}	612.21	612.21	612.21	612.21
Crystal size/mm^3	0.19 × 0.13 × 0.06	0.21 × 0.19 × 0.16	0.20 × 0.20 × 0.20	0.30 × 0.30 × 0.30
Temperature/K	203(2)	95(2)	296(2)	296(2)
θ range/° (completeness)	2.11–25.84(100%)	2.13–25.08(99.6%)	2.09–25.18(99.2%)	2.08–25.14(99.8%)
h; k; l range	−10, 13; ±18; −11, 9	±12; ±18; −11, 10	±12; ±18; ±11	±12; ±18; ±11
Crystal system	Orthorhombic	Orthorhombic	Orthorhombic	Orthorhombic
Space group	$P2_12_12$ (no. 18)	$P2_12_12$ (no. 18)	$P2_12_12$ (no. 18)	$P2_12_12$ (no. 18)
a/Å	10.6824(10)	10.7155(5)	10.6662(16)	10.6477(14)
b/Å	15.2673(13)	15.2302(8)	15.3354(19)	15.3321(15)
c/Å	9.6381(7)	9.5786(5)	9.764(3)	9.7742(19)
α/°	90	90	90	90
β/°	90	90	90	90
γ/°	90	90	90	90
V/Å^3	1571.9(2)	1563.22(14)	1597.1(5)	1595.7(4)
Z	2	2	2	2
D_{calc}/g cm^{-3}	1.293	1.301	1.273	1.274
μ (Mo Kα)/mm^{-1}	0.730	0.735	0.719	0.720
F(000)	638	638	638	638
Max./min. transmission	0.9547/0.8755	0.7452/0.6225	0.8696/0.8696	0.8131/0.8131
Reflections collected	10 368	9899	13 259	13 900
Independent reflect. (R_{int})	3038 (0.0571)	2774 (0.0188)	2859 (0.0849)	2856 (0.0939)
Data/restraints/parameters	3038/0/196	2774/0/196	2859/0/196	2856/0/196
Max./min. $\Delta\rho$/e Å^{-3} [a]	0.691/−0.481	1.607/−0.245[e]	2.327/−1.4185	0.590/−0.483
R_1/wR_2 [$I > 2\sigma(I)$][b]	0.0478/0.1091	0.0310/0.0846	0.0874/0.2159	0.0457/0.1136
R_1/wR_2 (all data)[b]	0.0618/0.1177	0.0325/0.0853	0.0977/0.2297	0.0558/0.1198
Goodness-of-fit on F^2[c]	1.064	1.070	1.099	1.013
Flack parameter[d]	0.02(2)	0.042(14)	0.07(4)	0.04(2)

[a] Largest difference peak and hole. [b] $R_1 = [\sum(||F_o| - |F_c||)/\sum|F_o|]$; $wR_2 = [\sum[w(F_o^2 - F_c^2)^2]/\sum[w(F_o^2)^2]]^{1/2}$. [c] Goodness-of-fit = $[\sum[w(F_o^2 - F_c^2)^2]/(n - p)]^{1/2}$. [d] Absolute structure parameter.[25] [e] We could refine the largest residual Q1 peak to an oxygen atom (of a presumed crystal water molecule) with an occupation factor of 0.13 per formula unit and further improve R-factors R_1, wR_2 (all data) of 0.0286/0.0752. In view of the calculated total potential solvent volume of 32–90 Å^3 or 2.1–5.6% in the **Cu-L1** structures (by PLATON,[41] see Table S3 in ESI†) a water molecule of crystallization might have been almost fully lost upon crystal drying. The presence or absence of small amounts of crystal water can have little structural effect.[57] A hydrogen-bonded H_2O molecule requires about 40 Å^3. For the data set of CuRL1a a freshly prepared crystal was used. In the CuR12 data set and in the room temperature data sets of Cu-*S*-L1 no significant residual electron was found in the voids.

state CD calculations were performed using Gaussian09.[54] All quantum-mechanics calculations were run on open-shell systems (charge 0, multiplicity 2).

Initial structures were generated starting from the available X-ray structure of the **Λ-Cu-*R*-L1** complex (Fig. 2). An initial structure with opposite configuration at the metal, **Δ-Cu-*R*-L1**, was obtained by mirror inversion of the whole complex, followed by manual inversion of the carbon chirality centers only. A simplified model was also obtained by replacing the 2-phenylethyl group by a methyl and optimizing the whole structure with DFT at the B3LYP/6-31G(d) level. Conformational searches were run with molecular mechanics, using the molecular Merck force field (MMFF). The geometry around the metal was kept fixed by constraining the O–Cu and N–Cu bond lengths and the O–Cu–O and N–Cu–N bond angles at their respective X-ray values. All the remaining rotatable bonds were included in the conformational search (*i.e.*, varied systematically) and optimized with MMFF. All structures thus obtained were fully re-optimized with DFT using both B3LYP and M06 functionals and the 6-31G(d) basis set on all atoms.[55]

Excited state calculations were run using the TDDFT method. A preliminary set of calculations was run on the simplified model described above to test the performance of various DFT functionals and basis sets. The following functionals were tested: B3LYP, CAM-B3LYP, BPV86, M06, and the two basis sets SVP and TZVP.[55] The calculation results were compared with the UV-vis and CD profiles of the series of Cu complexes, and the best results in terms of overall agreement were observed with M06/TZVP. M06/TZVP calculations were run on DFT optimized structures of both **Λ-Cu-*R*-L1** and **Δ-Cu-*R*-L1** complexes, considering two low-energy minima in both cases. The impact of the method used for the geometry optimizations was investigated by running TDDFT calculations on both B3LYP/6-31G(d) and M06/6-31G(d) optimized structures. The best combination (*i.e.* leading to better agreement with experimental UV-vis and CD profiles) was observed to be M06/TZVP//B3LYP/6-31G(d). In each TDDFT calculation, 72 excited states (roots) were considered. The spectra were generated using the program SpecDis[56] by applying a Gaussian band shape with 0.15 eV exponential half-width. Rotational strengths calculated with the dipole-length gauge were employed, the differences in dipole-velocity values being negligible for most transitions.

Table 6 Crystal data and structure refinement for **Cu-L2** and **Cu-L4**

Compound	**Λ/Δ-Cu-*R*-L2**	**Λ/Δ-Cu-*R*-L2**	**Λ-Cu-*R*-L4**
Data set	CuR14a	CuRL2-LT	CuRL4
Empirical formula	$C_{40}H_{36}CuN_2O_4$ [e]	$C_{40}H_{36}CuN_2O_4$ [e]	$C_{38}H_{30}Br_2CuN_2O_2$
M/g mol^{-1}	672.25	672.25	770.00
Crystal size/mm^3	0.18 × 0.15 × 0.08	0.30 × 0.30 × 0.10	0.30 × 0.03 × 0.03
Temperature/K	203(2)	100(2)	120(2)
θ range/° (completeness)	1.52–29.99(99.8%)	1.53–25.21(98.9%)	1.88–28.08(97.6%)
h; k; l range	±14; ±17; ±18	±12; ±14; −15, 16	±21; ±7; ±22
Crystal system	Triclinic	Triclinic	Monoclinic
Space group	$P1$ (no. 1)	$P1$ (no. 1)	$P2_1$ (no. 4)
a/Å	10.4041(8)	10.3705(13)	16.146(5)
b/Å	12.3307(9)	12.2802(16)	5.602(3)
c/Å	13.4434(11)	13.3595(16)	17.357(6)
α/°	89.643(4)	88.882(9)	90
β/°	83.777(4)	83.365(9)	99.10(3)
γ/°	74.684(4)	74.444(8)	90
V/Å^3	1653.1(2)	1627.9(4)	1550.1(10)
Z	2	2	2
D_{calc}/g cm^{-3}	1.351	1.371	1.650
μ (Mo Kα)/mm^{-1}	0.706	0.716	3.321
F(000)	702	702	774
Max./min. transmission	0.948/0.882	0.9318/0.8138	0.907/0.436
Reflections collected	39 828	14 496	17 213
Independent reflect. (R_{int})	18 019 (0.0782)	11 261 (0.0362)	7353 (0.0433)
Data/restraints/parameters	18 019/3/855[f]	11 261/3/855[f]	7353/1/408[f]
Max./min. $\Delta\rho$/e Å^{-3}[a]	0.469/−0.379	0.434/−0.829	0.409/−0.574
R_1/wR_2 [$I > 2\sigma(I)$][b]	0.0431/0.0907	0.0477/0.0926	0.0326/0.0574
R_1/wR_2 (all data)[b]	0.0784/0.0784	0.0638/0.0996	0.0498/0.0610
Goodness-of-fit on F^2[c]	0.961	1.010	0.916
Flack parameter[d]	0.016(6)	0.02(1)	0.005(6)

[a] Largest difference peak and hole. [b] $R_1 = [\sum(||F_o| - |F_c||)/\sum|F_o|]$; $wR_2 = [\sum[w(F_o^2 - F_c^2)^2]/\sum[w(F_o^2)^2]]^{1/2}$. [c] Goodness-of-fit = $[\sum[w(F_o^2 - F_c^2)^2]/(n - p)]^{1/2}$. [d] Absolute structure parameter.[25] [e] The structure contains two independent molecules in the asymmetric unit. However, check cif calculated $Z = 2$ with the moiety and sum formula $C_{40}H_{36}CuN_2O_4$. [f] In certain non-centrosymmetric space groups the origin along unique polar directions needs to be fixed. The SHELXL-97 program automatically applies least-square restraints for origin fixing in polar space groups, that is, 3 for space group $P1$ and 1 for space group $P2_1$.[58]

Acknowledgements

This work was supported by the Ministry of Science and Technology (MOST), Dhaka, Bangladesh under the Project 2012/13. We acknowledge the "Wazed Miah Science Research Centre", Jahangirnagar University, Dhaka, Bangladesh for taking CV and elemental analysis data. We thank Dr Klaus Ditrich (ChiPros) at BASF AG, Ludwigshafen for providing the enantiopure (*R*- or *S*)-*N*-(Ar)ethylamines.

Notes and references

1 (*a*) E. C. Escudero-Adán, M. M. Belmonte, J. Benet-Buchholz and A. W. Kleij, *Org. Lett.*, 2010, **12**, 4592–4595; (*b*) W. Clegg, R. W. Harrington, M. North and R. Pasquale, *Chem.–Eur. J.*, 2010, **16**, 6828–6843; (*c*) Z.-X. Xu, Z.-T. Huang and C.-F. Chen, *Tetrahedron Lett.*, 2009, **50**, 5430–5433; (*d*) M. Shibasaki, M. Kanai, S. Matsunaga and N. Kumagai, *Acc. Chem. Res.*, 2009, **42**, 1117–1127; (*e*) J. Niemeyer, G. Kehr, R. Frohlich and G. Erker, *Dalton Trans.*, 2009, 3731–3741; (*f*) P. Adão, J. O. M. R. Maurya, U. Kumar and I. Correia, *Inorg. Chem.*, 2009, **48**, 3542–3561; (*g*) J.-J. Lee, F.-Z. Yang, Y.-F. Lin, Y.-C. Chang, K.-H. Yu, M.-C. Chang, G.-H. Lee, Y.-H. Liu, Y. Wang, S.-T. Liu and J.-T. Chen, *Dalton Trans.*, 2008, 5945–5956; (*h*) K. R. Jain, W. A. Herrmann and F. E. Kühn, *Coord. Chem. Rev.*, 2008, **252**, 556–568; (*i*) Z. Chu, W. Huang, L. Wang and S. Gou, *Polyhedron*, 2008, **27**, 1079–1092; (*j*) D. Koth, M. Gottschaldt, H. Görls and K. Pohle, *Beilstein J. Org. Chem.*, 2006, **2**, 17; (*k*) C. T. Cohen, T. Chu and G. W. Coates, *J. Am. Chem. Soc.*, 2005, **127**, 10869–10878; (*l*) X. Zhou, J. Zhao, A. M. Santos and F. E. Kuehn, *Z. Naturforsch., B: Chem. Sci.*, 2004, **59**, 1223–1228; (*m*) G. Santoni and D. Rehder, *J. Inorg. Biochem.*, 2004, **98**, 758–764; (*n*) G. M. Sammis, H. Danjo and E. N. Jacobsen, *J. Am. Chem. Soc.*, 2004, **126**, 9928–9929; (*o*) J. F. Larrow and E. N. Jacobsen, *Top. Organomet. Chem.*, 2004, **6**, 123–152; (*p*) R. Dreos, G. Nardin, L. Randaccio, P. Siega and G. Tauzher, *Inorg. Chem.*, 2004, **43**, 3433–3440; (*q*) P. G. Cozzi, *Chem. Soc. Rev.*, 2004, **33**, 410–421; (*r*) G. M. Sammis and E. N. Jacobsen, *J. Am. Chem. Soc.*, 2003, **125**, 4442–4443; (*s*) O. V. Larionov, T. F. Savel'eva, K. A. Kochetkov, N. S. Ikonnokov, S. I. Kozhushkov, D. S. Yufit, J. A. K. Howard, V. N. Khrustalev, Y. N. Belokon and A. de Meijere, *Eur. J. Org. Chem.*, 2003, 869–877; (*t*) H. Gröger, *Chem. Rev.*, 2003, **103**, 2795–2828; (*u*) C.-M. Che and J.-S. Huang, *Coord. Chem. Rev.*, 2003, **242**, 97–113.

2 (*a*) B. Wisser, Y. Lu and C. Janiak, *Z. Anorg. Allg. Chem.*, 2007, **633**, 1189–1192; (*b*) B. Wisser and C. Janiak, *Z. Anorg. Allg. Chem.*, 2007, **633**, 1796–1800; (*c*) S. Klingelhöfer, M. Wiebcke and P. Behrens, *Z. Anorg. Allg. Chem.*, 2007, **633**, 113–119; (*d*) T. Ederer, R. S. Herrick and W. Beck, *Z. Anorg. Allg. Chem.*, 2007, **633**, 235–238; (*e*) T. Hauck, K. Sünkel and W. Beck, *Z. Anorg. Allg. Chem.*, 2006, **632**, 2305–2309.

3 (*a*) M. J. Plater, T. Gelbrich, M. B. Hursthouse and B. M. D. Silva, *CrystEngComm*, 2006, **8**, 895–903; (*b*) S. George, S. Lipstman, S. Muniappan and I. Goldberg, *CrystEngComm*, 2006, **8**, 417–424; (*c*) R. Urban and W. Beck, *Z. Naturforsch., B: Chem. Sci.*, 2005, **60**, 1071–1076; (*d*) B. Paul, C. Näther, K. M. Fromm and C. Janiak, *CrystEngComm*, 2005, **7**, 309–319; (*e*) W. Hoffmueller, H. Dialer and W. Beck, *Z. Naturforsch., B: Chem. Sci.*, 2005, **60**, 1278–1286.

4 (*a*) R. Urban, D. Veghini, H. Berke and W. Beck, *Z. Anorg. Allg. Chem.*, 2005, **631**, 2715–2718; (*b*) G. Müller and J. Brand, *Z. Anorg. Allg. Chem.*, 2005, **631**, 2820–2829; (*c*) T. J. Colacot and N. S. Hosmane, *Z. Anorg. Allg. Chem.*, 2005, **631**, 2659–2668; (*d*) H. Brunner and C. Keck, *Z. Anorg. Allg. Chem.*, 2005, **631**, 2555–2562; (*e*) H. Brunner and H. Leyerer, *J. Organomet. Chem.*, 1987, **334**, 369–376; (*f*) H. Brunner and H. Fisch, *J. Organomet. Chem.*, 1987, **335**, 1–14.

5 (*a*) C. P. Pradeep and S. K. Das, *Polyhedron*, 2009, **28**, 630–636; (*b*) C. P. Pradeep, P. S. Zacharias and S. K. Das, *Inorg. Chem. Commun.*, 2008, **11**, 89–93; (*c*) C. P. Pradeep, P. S. Zacharias and S. K. Das, *Eur. J. Inorg. Chem.*, 2007, 5377–5389; (*d*) C. P. Pradeep, P. S. Zacharias and S. K. Das, *Eur. J. Inorg. Chem.*, 2005, 3405–3408; (*e*) C. P. Pradeep, T. Htwe, P. S. Zacharias and S. K. Das, *New J. Chem.*, 2004, **28**, 735–739; (*f*) R. Fleischer, H. Wunderlich and M. Braun, *Eur. J. Org. Chem.*, 1998, 1063–1070.

6 (*a*) C. Evans and D. Luneau, *J. Chem. Soc., Dalton Trans.*, 2002, 83–86; (*b*) H. Sakiyama, H. Okawa, N. Matsumoto and S. Kida, *Bull. Chem. Soc. Jpn.*, 1991, **64**, 2644–2647; (*c*) H. Sakiyama, H. Okawa, N. Matsumoto and S. Kida, *J. Chem. Soc., Dalton Trans.*, 1990, 2935–2939; (*d*) H. Ōkawa, M. Nakamura and S. Kida, *Inorg. Chim. Acta*, 1986, **120**, 185–189.

7 (*a*) T. Akitsu, *Polyhedron*, 2007, **26**, 2527–2535; (*b*) T. Akitsu and Y. Einaga, *Polyhedron*, 2006, **25**, 1089–1095; (*c*) T. Akitsu and Y. Einaga, *Polyhedron*, 2005, **24**, 2933–2943; (*d*) T. Akitsu and Y. Einaga, *Polyhedron*, 2005, **24**, 1869–1877; (*e*) T. Akitsu and Y. Einaga, *Acta Crystallogr., Sect. C: Cryst. Struct. Commun.*, 2004, **60**, m640–m642; (*f*) G.-P. Li, Q.-C. Yang, Y.-Q. Tang, Y.-D. Guan and Z.-H. Shang, *Acta Chim. Sin.*, 1987, **45**, 421–425.

8 (*a*) H. Brunner, T. Zwack, M. Zabel, W. Beck and A. Böhm, *Organometallics*, 2003, **22**, 1741–1750; (*b*) H. Brunner, R. Oeschey and B. Nuber, *J. Chem. Soc., Dalton Trans.*, 1996, 1499–1508; (*c*) S. K. Mandal and A. R. Chakravarty, *J. Chem. Soc., Dalton Trans.*, 1992, 1627–1633; (*d*) S. K. Mandal and A. R. Chakravarty, *J. Organomet. Chem.*, 1991, **417**, C59–C62.

9 (*a*) C. Gan, G. Lai, Z. Zhang, Z. Wang and M.-M. Zhou, *Tetrahedron: Asymmetry*, 2006, **17**, 725–728; (*b*) M. Itagaki, K. Hagiya, M. Kamitamari, K. Masumoto, K. Suenobu and Y. Yamamoto, *Tetrahedron*, 2004, **60**, 7835–7843; (*c*) Z. Li, G. Liu, Z. Zheng and H. Chen, *Tetrahedron*, 2000, **56**, 7187–7191.

10 (*a*) R. D. Chakravarthy, K. Suresh, V. Ramkumar and D. K. Chand, *Inorg. Chim. Acta*, 2011, **376**, 57–63; (*b*) C. Zhang, G. Rheinwald, V. Lozan, B. Wu, P.-G. Lassahn, H. Lang and C. Janiak, *Z. Anorg. Allg. Chem.*, 2002, **628**, 1259–1268; (*c*) L. Z. Flores-Lopéz, M. Parra-Hake, R. Somanathan and P. J. Walsh, *Organometallics*, 2000, **19**, 2153–2160; (*d*) H. Brunner, M. Niemetz and M. Zabel, *Z. Naturforsch., B: Chem. Sci.*, 2000, **55**, 145–154; (*e*) S. Prasad Rath, T. Ghosh and S. Mondal, *Polyhedron*, 1997, **16**, 4179–4186.

11 (*a*) A. Zulauf, M. Mellah, X. Hong and E. Schulz, *Dalton Trans.*, 2010, **39**, 6911–6935; (*b*) L.-L. Lin, X.-H. Liu and X.-M. Feng, *Prog. Chem.*, 2010, **22**, 1353–1361; (*c*) K. C. Gupta, A. Kumar Sutar and C.-C. Lin, *Coord. Chem. Rev.*, 2009, **253**, 1926–1946; (*d*) S. H. R. Abdi, R. I. Kureshy, N. H. Khan, V. J. Mayani and H. C. Bajaj, *Catal. Surv. Asia*, 2009, **13**, 104–131; (*e*) K. C. Gupta and A. K. Sutar, *Coord. Chem. Rev.*, 2008, **252**, 1420–1450; (*f*) K. Matsumoto, B. Saito and T. Katsuki, *Chem. Commun.*, 2007, 3619–3627.

12 D. Koch, W. Hoffmuller, K. Polborn and W. Beck, *Z. Naturforsch., B: Chem. Sci.*, 2001, **56**, 403–410.

13 (*a*) I. Karamé, M. Jahjah, A. Messaoudi, M. L. Tommasino and M. Lemaire, *Tetrahedron: Asymmetry*, 2004, **15**, 1569–1581; (*b*) I. Karamé, M. L. Tommasino, R. Faure and M. Lemaire, *Eur. J. Org. Chem.*, 2003, 1271–1276.

14 (*a*) Z.-H. Yang, L.-X. Wang, Z.-H. Zhou, Q.-L. Zhou and C.-C. Tang, *Tetrahedron: Asymmetry*, 2001, **12**, 1579–1582; (*b*) P. Guo and K.-Y. Wong, *Electrochem. Commun.*, 1999, **1**, 559–563; (*c*) E. D. McKenzie and S. J. Selvey, *Inorg. Chim. Acta*, 1985, **101**, 127–133.

15 A. L. Iglesias, G. Aguirre, R. Somanathan and M. Parra-Hake, *Polyhedron*, 2004, **23**, 3051–3062.

16 (*a*) M. Enamullah, A. K. M. Royhan Uddin, G. Hogarth and C. Janiak, *Inorg. Chim. Acta*, 2012, **387**, 173–180; (*b*) C. Janiak, A.-C. Chamayou, A. K. M. Royhan Uddin, M. Uddin, K. S. Hagen and M. Enamullah, *Dalton Trans.*, 2009, 3698–3709; (*c*) M. Enamullah, U. A. K. M. Royhan, A.-C. Chamayou and C. Janiak, *Z. Naturforsch., B: Chem. Sci.*, 2007, **62**, 807–817.

17 (*a*) M. Enamullah, *J. Coord. Chem.*, 2011, **64**, 1608–1616; (*b*) M. Enamullah, *J. Coord. Chem.*, 2012, **65**, 911–922.

18 (*a*) A. von Zelewsky, *Stereochemistry of Coordination Compounds*, John Wiley & Sons, Chichester, 1996, p. 69; (*b*) H. Amouri and M. Gruselle, *Chirality in Transition Metal Chemistry: Molecules, supramolecular assemblies and materials*, John Wiley & Sons, Chichester, 2008, pp. 40–41; (*c*) K. A. Jensen, *Inorg. Chem.*, 1970, **9**, 1–5.

19 A.-C. Chamayou, S. Lüdeke, V. Brecht, T. B. Freedman, L. A. Nafie and C. Janiak, *Inorg. Chem.*, 2011, **50**, 11363–11374.

20 R. E. Ernst, M. J. O'Connor and R. H. Holm, *J. Am. Chem. Soc.*, 1967, **89**, 6104–6113.
21 (*a*) M. Enamullah, V. Vasylyeva and C. Janiak, *Inorg. Chim. Acta*, 2013, **408**, 109–119; (*b*) M. Enamullah and M. K. Islam, *J. Coord. Chem.*, 2013, **66**, 4107–4118.
22 R. S. Downing and F. L. Urbach, *J. Am. Chem. Soc.*, 1969, **91**, 5977–5983.
23 S. E. Howson, L. E. N. Allan, N. P. Chmel, G. J. Clarkson, R. van Gorkum and P. Scott, *Chem. Commun.*, 2009, 1727–1729; A. von Zelewsky and O. Mamula, *J. Chem. Soc., Dalton Trans.*, 2000, 219–231.
24 J. M. Becker, J. Barker, G. J. Clarkson, R. van Gorkum, G. K. Johal, R. I. Walton and P. Scott, *Dalton Trans.*, 2010, **39**, 2309–2326.
25 (*a*) H. D. Flack, M. Sadki, A. L. Thompson and D. J. Watkin, *Acta Crystallogr., Sect. A: Fundam. Crystallogr.*, 2011, **67**, 21–34; (*b*) H. D. Flack and G. Bernardinelli, *Chirality*, 2008, **20**, 681–690; (*c*) H. D. Flack and G. Bernardinelli, *Acta Crystallogr., Sect. A: Fundam. Crystallogr.*, 1999, **55**, 908–915; (*d*) H. Flack, *Acta Crystallogr., Sect. A: Fundam. Crystallogr.*, 1983, **39**, 876–881.
26 E. F. Paulus and A. Gieren, in *Handbook of Analytical Techniques*, Wiley-VCH Verlag GmbH, New York, 2001, vol. 1, pp. 373–417.
27 I. Kalf, B. Calmuschi and U. Englert, *CrystEngComm*, 2002, **4**, 548–551 and references therein.
28 *Comprehensive Chiroptical Spectroscopy*, ed. N. Berova, R. W. Woody, P. Polavarapu and K. Nakanishi, Wiley, New York, 2012.
29 (*a*) G. Pescitelli, L. Di Bari and N. Berova, *Chem. Soc. Rev.*, 2011, **40**, 4603–4625; (*b*) N. Berova, L. Di Bari and G. Pescitelli, *Chem. Soc. Rev.*, 2007, **36**, 914–931.
30 B. Bosnich, *J. Am. Chem. Soc.*, 1968, **90**, 627–632.
31 S. Yamada, *Coord. Chem. Rev.*, 1999, **190–192**, 537–555.
32 G.-J. M. Fernández, E. Acevedo-Arauz, R. Cetina-Rosado, R. A. Toscano, N. Macías-Ruvalcaba and M. Aguilar-Martínez, *Transition Met. Chem.*, 1999, **24**, 18–24.
33 (*a*) J. Fernández-G, O. Ruíz-Ramírez, R. Toscano, N. Macías-Ruvalcaba and M. Aguilar-Martínez, *Transition Met. Chem.*, 2000, **25**, 511–517; (*b*) G. S. Patterson and R. H. Holm, *Bioinorg. Chem.*, 1975, **4**, 257–275.
34 J. M. Fernández-G, C. Ausbun-Valdés, E. E. González-Guerrero and R. A. Toscano, *Z. Anorg. Allg. Chem.*, 2007, **633**, 1251–1256.
35 Y. Shibuya, K. Nabari, M. Kondo, S. Yasue, K. Maeda, F. Uchida and H. Kawaguchi, *Chem. Lett.*, 2008, **37**, 78–79.
36 L. Yang, D. R. Powell and R. P. Houser, *Dalton Trans.*, 2007, 955–964.
37 A. W. Addison, T. N. Rao, J. Reedijk, J. van Rijn and G. C. Verschoor, *J. Chem. Soc., Dalton Trans.*, 1984, 1349–1356.
38 K. Brandenburg *Diamond (Version 3.2), Crystal and Molecular Structure Visualization*, Crystal Impact – K. Brandenburg & H. Putz Gbr, Bonn, Germany, 2009.
39 (*a*) B. Gil-Hernandez, H. A. Hoppe, J. K. Vieth, J. Sanchiz and C. Janiak, *Chem. Commun.*, 2010, **46**, 8270–8272; (*b*) H. Flack, *Acta Crystallogr., Sect. A: Fundam. Crystallogr.*, 2009, **65**, 371–389; (*c*) M. Enamullah, A. Sharmin, M. Hasegawa, T. Hoshi, A.-C. Chamayou and C. Janiak, *Eur. J. Inorg. Chem.*, 2006, 2146–2154.
40 (*a*) M. Nishio, *Phys. Chem. Chem. Phys.*, 2011, **13**, 13873–13900; (*b*) M. Nishio, Y. Umezawa, K. Honda, S. Tsuboyama and H. Suezawa, *CrystEngComm*, 2009, **11**, 1757–1788; (*c*) X.-J. Yang, F. Drepper, B. Wu, W.-H. Sun, W. Haehnel and C. Janiak, *Dalton Trans.*, 2005, 256–267 and supplementary material therein (*d*) M. Nishio, *CrystEngComm*, 2004, **6**, 130–158; (*e*) C. Janiak, S. Temizdemir, S. Dechert, W. Deck, F. Girgsdies, J. Heinze, M. J. Kolm, T. G. Scharmann and O. M. Zipffel, *Eur. J. Inorg. Chem.*, 2000, 1229–1241; (*f*) C. Janiak, *J. Chem. Soc., Dalton Trans.*, 2000, 3885–3896; (*g*) Y. Umezawa, S. Tsuboyama, K. Honda, J. Uzawa and M. Nishio, *Bull. Chem. Soc. Jpn.*, 1998, **71**, 1207–1213; (*h*) M. Nishio, M. Hirota and Y. Umezawa, *The CH/π interaction (evidence, nature and consequences)*, Wiley-VCH, New York, 1998.
41 (*a*) A. Spek, *Acta Crystallogr., Sect. D: Biol. Crystallogr.*, 2009, **65**, 148–155; (*b*) A. L. Spek, *PLATON – A multipurpose crystallographic tool*, Utrecht University, Utrecht, The Netherlands, 2005.
42 (*a*) A. Kelch, I. Dix, H. Hopf and P. G. Jones, *Acta Crystallogr., Sect. C: Cryst. Struct. Commun.*, 2013, **69**, 627–629; (*b*) P. G. Jones and P. Kus, *Z. Naturforsch., B: Chem. Sci.*, 2010, **65**, 433–444; (*c*) V. R. Pedireddi, D. S. Reddy, B. S. Goud, D. C. Craig, A. D. Rae and G. R. Desiraju, *J. Chem. Soc., Perkin Trans. 2*, 1994, 2353–2360.
43 A. I. Kitaigorodskii, *Molecular Crystals and Molecules*, Academic Press, New York, 1973.
44 (*a*) G. Pescitelli, T. Kurtán and K. Krohn, in *Comprehensive Chiroptical Spectroscopy*, ed. N. Berova, R. W. Woody, P. Polavarapu and K. Nakanishi, Wiley, New York, 2012, vol. 2, pp. 217–249; (*b*) G. Pescitelli, T. Kurtán, U. Flörke and K. Krohn, *Chirality*, 2009, **21**, E181–E201.
45 (*a*) J. Autschbach, in *Comprehensive Chiroptical Spectroscopy*, ed. N. Berova, R. W. Woody, P. Polavarapu and K. Nakanishi, Wiley, New York, 2012, vol. 1, pp. 593–642; (*b*) H. Cox and A. J. Stace, *Int. Rev. Phys. Chem.*, 2010, **29**, 555–588.
46 (*a*) J. M. Dragna, G. Pescitelli, L. Tran, V. M. Lynch, E. V. Anslyn and L. Di Bari, *J. Am. Chem. Soc.*, 2012, **134**, 4398–4407; (*b*) L. You, G. Pescitelli, E. V. Anslyn and L. Di Bari, *J. Am. Chem. Soc.*, 2012, **134**, 7117–7125.
47 A. Ipatov, F. Cordova, L. J. Doriol and M. E. Casida, *J. Mol. Struct. (THEOCHEM)*, 2009, **914**, 60–73.
48 Y. Zhao and D. Truhlar, *Theor. Chem. Acc.*, 2008, **119**, 525–525.
49 (*a*) G. Pescitelli, D. Padula and F. Santoro, *Phys. Chem. Chem. Phys.*, 2013, **15**, 795–802; (*b*) D. Padula, S. Di Pietro, M. A. M. Capozzi, C. Cardellicchio and G. Pescitelli, *Chirality*, 2013, DOI: 10.1002/chir.22270.
50 *APEX2, data collection program for the CCD area-detector system, Version 2.1-0*, Bruker Analytical X-ray Systems, Madison (WI), 2006.

51 *SAINT, data reduction and frame integration program for the CCD area-detector system*, Bruker Analytical X-ray Systems, Madison (WI), 2006.
52 G. Sheldrick, *Acta Crystallogr., Sect. A: Fundam. Crystallogr.*, 2008, **64**, 112–122.
53 G. M. Sheldrick, *Program SADABS*, University of Göttingen, Göttingen, Germany, 1996.
54 M. J. Frisch, G. W. Trucks, H. B. Schlegel, G. E. Scuseria, M. A. Robb, J. R. Cheeseman, G. Scalmani, V. Barone, B. Mennucci, G. A. Petersson, H. Nakatsuji, M. Caricato, X. Li, H. P. Hratchian, A. F. Izmaylov, J. Bloino, G. Zheng, J. L. Sonnenberg, M. Hada, M. Ehara, K. Toyota, R. Fukuda, J. Hasegawa, M. Ishida, T. Nakajima, Y. Honda, O. Kitao, H. Nakai, T. Vreven, J. A. Montgomery, J. E. Peralta, F. Ogliaro, M. Bearpark, J. J. Heyd, E. Brothers, K. N. Kudin, V. N. Staroverov, R. Kobayashi, J. Normand, K. Raghavachari, A. Rendell, J. C. Burant, S. S. Iyengar, J. Tomasi, M. Cossi, N. Rega, J. M. Millam, M. Klene, J. E. Knox, J. B. Cross, V. Bakken, C. Adamo, J. Jaramillo, R. Gomperts, R. E. Stratmann, O. Yazyev, A. J. Austin, R. Cammi, C. Pomelli, J. W. Ochterski, R. L. Martin, K. Morokuma, V. G. Zakrzewski, G. A. Voth, P. Salvador, J. J. Dannenberg, S. Dapprich, A. D. Daniels, Ö. Farkas, J. B. Foresman, J. V. Ortiz, J. Cioslowski and D. J. Fox, *GAUSSIAN 09 (Revision C.01)*, Wallingford CT, 2009.
55 All references about DFT functionals and basis sets can be found in the on-line documentation for Gaussian'09 at http://www.gaussian.com/g_tech/g_ur/g09help.htm
56 T. Bruhn, A. Schaumlöffel, Y. Hemberger and G. Bringmann, *Chirality*, 2013, **25**, 243–249.
57 H. H. Monfared, A.-C. Chamayou, S. Khajeh and C. Janiak, *CrystEngComm*, 2010, **12**, 3526–3530.
58 H. D. Flack and D. Schwarzenbach, *Acta Crystallogr., Sect. A: Fundam. Crystallogr.*, 1988, **44**, 499–506.